Swansea University
Prifysgol Abertawe

Optimisation and Exploration of Inkjet Printing in Triple Mesoscopic Perovskite Cells

By
Alice Eleanor Bridget Armstrong

Submitted to Swansea University
in fulfilment of the requirements for the degree of
MSc in Materials Engineering by Research

Swansea University
2025

Summary of Research

Silicon is used as the key component in commercial Photovoltaic Cell fabrication today. It has enabled the production of efficient, stable devices with power conversion efficiencies (PCE) of around 25% and a serviceable lifetime of up to 25 years. [1] To achieve these results the Silicon has to be pure without structural defects making them expensive to produce.

Perovskite offers a potentially more flexible and easy to produce alternative that is more tolerant to imperfections and impurities. Perovskites need to be ultra-thin to enhance performance, and recent lab based PCEs approaching those of silicon have been achieved. [1] The main drawback has been the long-term stability due to reaction of the perovskite with water making them sensitive to moisture ingress and humidity. This has been addressed by the carbon stack printable cell geometry used in this research. [2] This uses readily available materials – TiO_2 and ZrO_2 – that can be screen-printed to create the stack and has the additional advantage that they do not require expensive hole transport materials such as spiro-OMeTAD. [3]

This research builds on the carbon stack cell geometry and explores the feasibility of using inkjet printing for the deposition of the perovskite into the cell, which would assist in facilitating the upscaling of production from the manual methods used in lab research. It also explores the potential of non-hazardous precursor inks which would additionally contribute to the safety and a reduction in the cost of production.

To create the cell the perovskite has to infiltrate all layers of the carbon stack which requires optimisation of the droplet deposition parameters used in the inkjet-printing method. This research used the SUSS LP50 inkjet printer to determine the optimum characteristics of ink droplet deposition, and printer runs to create the best PCE for the cells. It also varied the concentrations and viscosity of the two inks studied – γ-butyrolactone (GBL) and γ-valerolactone (GVL) a less toxic substitute for GBL to produce results.

This research shows that the inkjet deposition of the perovskite into the carbon stack geometry can reliably produce cells with PCE of over 10%, it has also shown that the green alternative solvent GVL does not compromise the efficiency of the cell. Both of these novel approaches offer a promising way forward to commercial fabrication of large, safe, stable and efficient perovskite solar cells.

Acknowledgements

Firstly, I would like to thank Swansea University for allowing me to pursue this project.
I would also like to thank my supervisors Professor Trystan Watson and Dr Simoni Meroni who supported me throughout this project and who I enjoyed working with immensely.
I would also like to thank Dr Dimitrios Raptis and Carys Worsley who also provided me with support.
Particular thanks to Simoni for being so giving with your time and expertise without which this project would not have been possible.
Finally, thank you to my family and friends who have supported me throughout my research journey.

Declarations

This work has not previously been accepted in substance for any degree and is not being concurrently submitted in candidature for any degree.

Signed..... .....

Date: 19/03/2025.....

This thesis is the result of my own investigations, except where otherwise stated. Other sources are acknowledged by footnotes giving explicit references. A bibliography is appended.

Signed.....
Date: 19/03/2025.....

I hereby give consent for my thesis, if accepted, to be available for photocopying and for inter-library loan, and for the title and summary to be made available to outside organisations.

Signed.....
Date: 19/03/2025.....

The University's ethical procedures have been followed and, where appropriate, that ethical approval has been granted.

Signed.....

Date: 19/03/2025.....

Table of Contents

i. List of tables and figures

1.0 Introduction

Perovskite solar cells are thin-film devices manufactured with a layered structure. This structure can be either printed using liquid inks or vacuum-deposited. The perovskite is then infiltrated into this layered structure. Producing uniform, high-performance perovskite material in a large-scale manufacturing environment is difficult, and there is a substantial difference in small-area cell efficiency and large-area module efficiency. The future of perovskite manufacturing will depend on solving this challenge.

The aims of this body of research were to assess the suitability of inkjet printing as a deposition method for perovskite precursor onto the mesoscopic carbon stack structure – a particular geometry of cell - and to discover whether the green solvent systems utilised would produce inks suitable for this method of manufacture. This was carried out with the aim of optimising a production method that compliments the screen printed layers of the carbon stack and could in future be used for scaled up devices while still providing cells with efficiency standards comparable to the established method for perovskite deposition at the solar cell scale i.e. pipette deposition.

In this thesis the novel method of inkjet printing for perovskite deposition is considered as a potential technique for use in the manufacturing of triple mesoscopic perovskite solar cells. The suitability of the methylammonium lead iodide (MAPI) perovskite precursor as well as two different green solvent systems, GBL and GVL, is examined as well as the suitability of the technique overall.

The first portion of this research examined the precursor inks and worked to optimise these for use with the inkjet printer. Analysis of the viscosity of both the GBL and GVL solvents was carried out. Furthermore, the two perovskite ‘inks’ (MAPI GBL and MAPI GVL) were studied to compare the performance of the solvents in both perovskite solutions. The results of this viscosity testing then informed the work done with the inks using the inkjet printer which consisted of advanced drop analysis carried out using the PiXDRO software. This advanced drop analysis (ADA) assessed the ink droplets falling from the printhead using a camera.

The second portion of this research explored the suitability of inkjet printing of the perovskite precursor as a method of deposition for the carbon mesoscopic solar cells. This was the selected architecture for the solar cell and comprised of three mesoscopic layers TiO_2, ZrO_2 and carbon top layer printed onto a glass substrate. The optimisation of this deposition process was also addressed by exploring different aspects of the process such as the size of the deposition area and the printhead speed, the volume of perovskite deposited as well as examining the 'post-print' processes.

To determine the success of these different parameters testing was done on a solar simulator to assess the efficiency of the cells produced. This also allowed for examination of the V_{OC}, J_{SC}, fill factor and therefore the efficiency of the cells which helped to determine whether the inkjet printer was a suitable method of deposition.

2.0 Literature Review

2.1 Perovskite Solar Cells

Silicon has been the most popular material in photovoltaic (PV) technology with 97% of commercial solar solutions utilising silicon. [4] This established use of silicon solar cells is due to the technology providing a combination of high efficiency with power conversion efficiencies (PCE) of 25-30% in commercial devices, at relatively low cost, and with a long lifetime. Commercial modules today are designed to have a 25-year warranty and are still capable of producing more than 80% of their original power after this time. [5]

Halide perovskites are a family of materials that have shown potential for high performance and low production costs in solar cells. Perovskite solar cells use raw materials that are cheap, abundant and easy to find all over the world. The manufacturing process for perovskite solar panels is also relatively simple and can be conducted at lower temperatures than that of traditional silicon panels. Perovskite solar cells use only a thin layer of perovskite material, which allows for lightweight and flexible panel designs. They could work well in a variety of innovative settings, including curved surfaces, building-integrated photovoltaics, and portable electronics.

Perovskite solar cells have shown remarkable progress in recent years with rapid increases in efficiency, from reports of about 3% in 2009 to over 25% today. [6]

An important property of PV semiconductors is the bandgap. This is the energy required for an electron to move from the valence to conduction band which indicates what wavelengths of light the material can absorb and convert to electrical energy. If the semiconductor's bandgap matches the wavelengths of light incident on the PV cell, then that cell can efficiently make use of all the available energy. This means the electrons in the cell absorb all the available light energy as the bandgap is the energy difference between the valence band and the conductive band. This would be the maximum efficiency for the cell, in reality light of varying wavelengths hits the surface of the cell therefore resulting in some being absorbed and some being reflected. Perovskite is much better at absorbing light than crystalline silicon and can even be 'tuned' to use regions of the solar spectrum largely inaccessible to silicon photovoltaics. [7]

The amount of electricity produced from PV cells depends on the characteristics (such as intensity and wavelengths) of the light available and multiple performance attributes of the cell. Perovskite solar cells (PSCs) conversion efficiencies can be more than 25%. They have however, been found to exhibit poor stability in long term ageing tests. [5]

Among different configurations of PSCs, the carbon stack mesoscopic perovskite cells which use the carbon counter electrode-based principle and do not use a hole transporting material (HTM) have proved interesting due to their promising characteristics.

2.2 The Carbon Stack

The carbon stack is an example of the perovskite solar cell architecture. It is a thin-film perovskite solar cell (PSC) structure which has been developed as an alternative to silicon technologies because it offers the opportunity for simple and scalable fabrication. [8]

The carbon stack consists of a glass substrate treated with a layer of compact titanium oxide (c-TiO_2), a screen-printed mesoporous electron transport layer of titanium oxide (TiO_2) a screen-printed mesoporous insulating layer of zirconia (ZrO_2) and a screen-printed porous conductive carbon top contact. [9]]

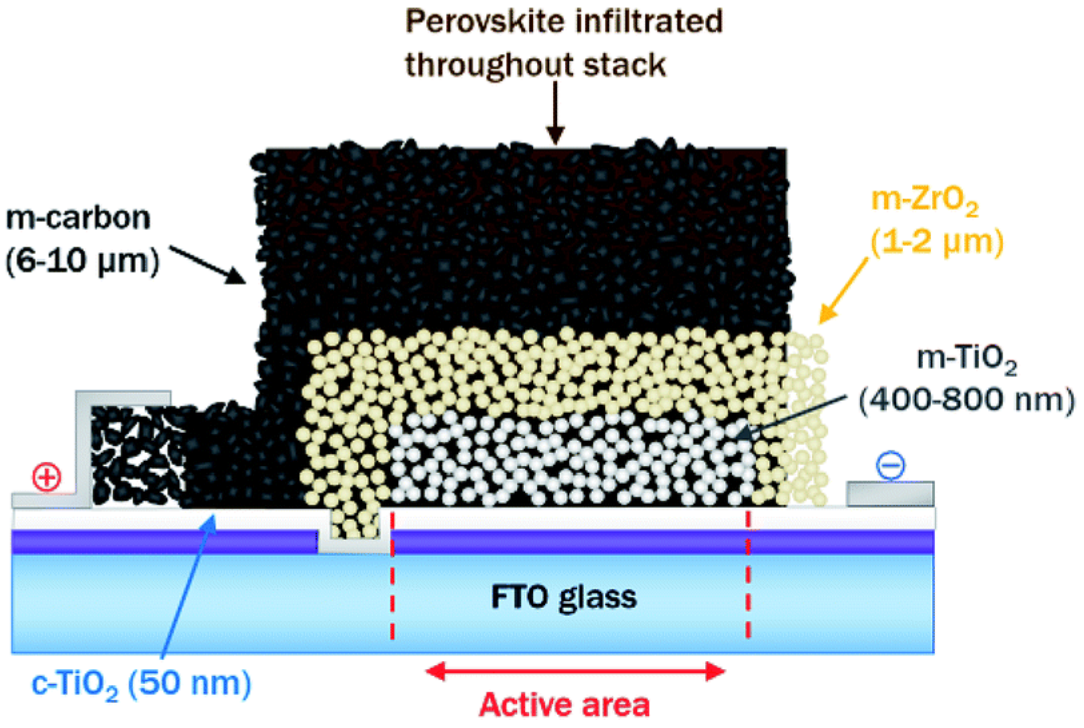

Figure 1 – Schematic of the structure of the mesoporous carbon stack [8]

This structure is then annealed at high temperature to remove the organic binders before the infiltration of the perovskite ink.

Using screen printing as the method of production for this structure also means that the technology is inherently scalable with the exception of the current methods used for the infiltration of the perovskite. As this technology is fully printable it incurs low capital costs, and the cells can be produced using inexpensive materials. This production method also limits the waste of materials used, when compared to pipette and spin coating.

There is no hole transport layer (HTL) in this structure meaning that the perovskite permeates and is 'hosted' by all three layers of the carbon stack. This is the major advantage with the triple layer carbon stack as the structure can be manufactured but not infiltrated and the stacks can be stored. The perovskite can then be infiltrated as needed to produce devices on demand.

For small scale individual cells, the infiltration method used for perovskite utilises an Eppendorf pipette to deposit the precursor onto the carbon stack. This method both limits the technology in terms of scale up and also poses problems in terms of the uniformity of the deposition of perovskite across the active area of the cell.

This advantage is compounded when the inkjet printer is introduced as the deposition method for the perovskite. The stacks can be pre prepared en masse and then infiltrated when needed on a larger scale than with the Eppendorf pipette method. This project aims to investigate the feasibility of using inkjet printing as a potential process by which the carbon stack can be infiltrated with the perovskite.
The method of inkjet printing has already been used as part of the manufacturing process of perovskite solar cells. [10] However, most of the work done with the inkjet so far has focused on using it as an alternative printing method for the mesoporous layers rather than for depositing the perovskite. If perovskites can be made reliably using these scalable fabrication approaches, they have the potential for faster capacity expansion than silicon PV. Both of these processes are well established in other industries, so existing knowledge and supply chains can be leveraged to further reduce scaling costs and risk.

While perovskite solar cells have become highly efficient in a very short time, a number of challenges remain before they can become a competitive commercial technology. The step that prohibits scale-up of carbon stack PSCs is the manual infiltration of the perovskite precursor solution. Upscaling may be possible if the manual infiltration of perovskite precursor step could be replaced with a mass reproducible technique such as inkjet printing.

2.3 Silicon vs Perovskites

Silicon is the most common semiconductor material used in the production of solar cells. The crystallised form is preferrable and most commonly used, as this material has demonstrated the highest power conversion efficiency (PCE). The material has to be extremely pure and not have any structural defects to work efficiently which drives up production costs. Silicon PV cells are fabricated at high temperatures and under vacuum conditions, making them expensive to produce. The upper limit of efficiency achieved for silicon PV cells has hovered at around 29%. See Figure 1.

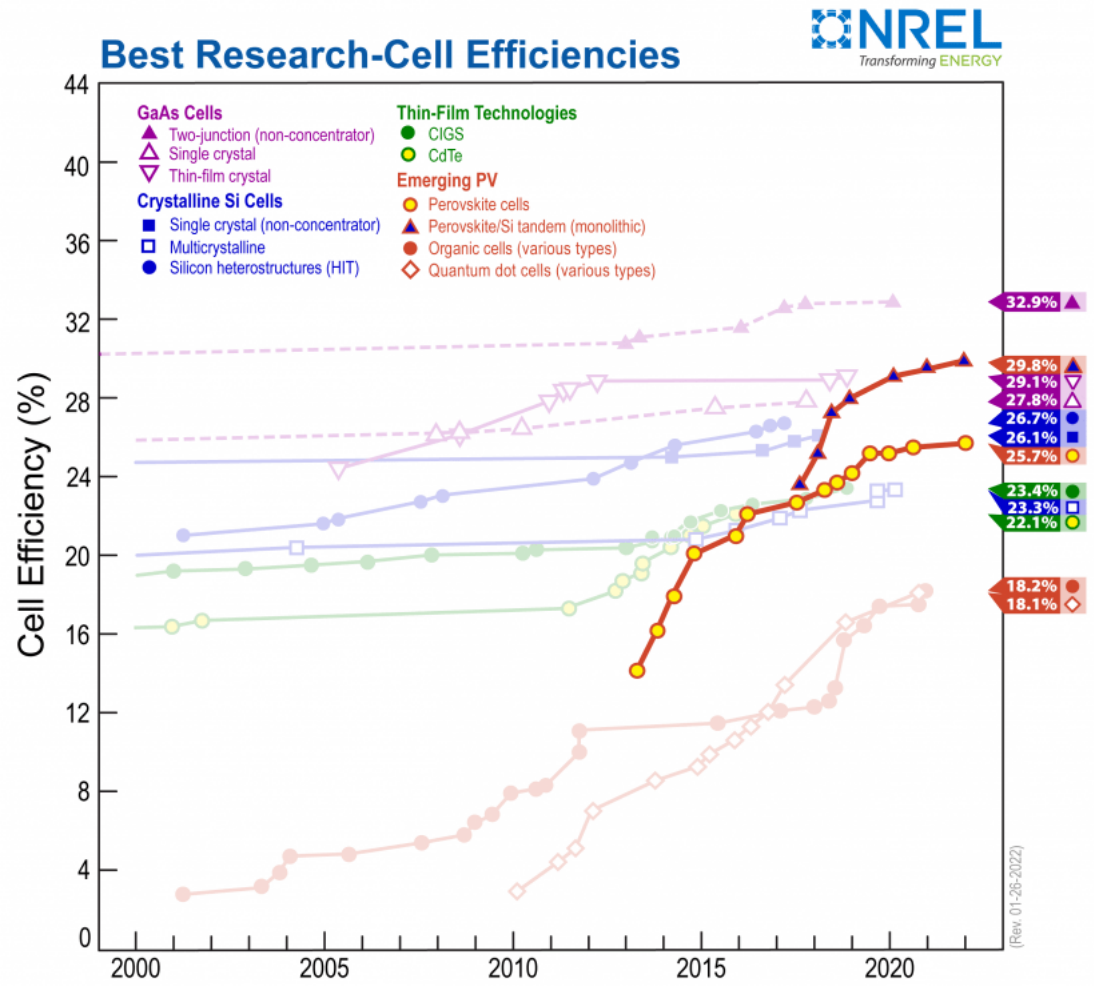

Figure 2- Efficiency records for perovskite PV cells compared to other PV technologies with current records of 25.7% for single junction perovskite devices and 29.8% for tandem perovskite-silicon devices (as of January 26, 2022). [1]

Perovskite is much better at absorbing light than silicon and can even be 'tuned' to use regions of the solar spectrum largely inaccessible to silicon photovoltaics. It also has a better tolerance for defects such as irregularities in the microstructure e.g. interstitials or atomic vacancies and can function well with impurities and imperfections. Perovskites can be produced more easily and with greater flexibility. This flexibility allows the perovskites to be rollable and printable unlike the rigid silicon cell. Perovskite cells are built with layers of materials that are printed, coated, or vacuum-deposited onto an underlying support layer, known as the substrate.

One drawback is the fact perovskites contain toxic lead. Consequently, researchers have been trying to find new, more stable perovskite materials and experimenting with different ways of optimising perovskites and their architecture in the creation of solar cells.

2.4 The Tandem Solar Cell: Perovskite on Silicon

One option for improving upon efficiency of solar cells that has been explored is to use stacked planar structures comprising different semiconductor materials — known as tandem photovoltaics.

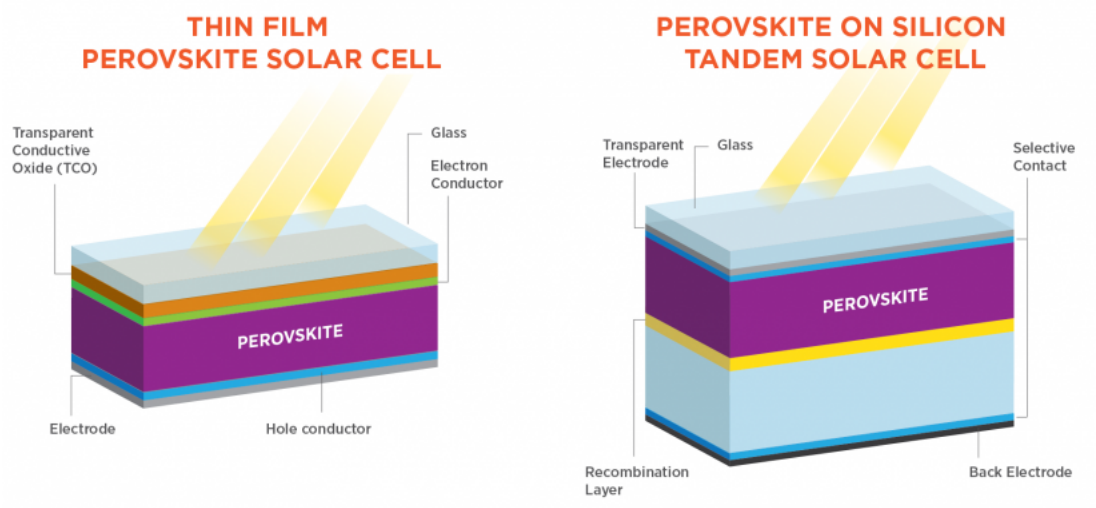

Figure 3 -Thin film perovskite solar cell structure vs tandem solar cell structure. Taken from the Office of Energy Efficiency and Renewable Energy [1]

Researchers realised that combining silicon and perovskite was a good way to go. The top perovskite cell absorbs high-energy photons, while the silicon-based bottom cell absorbs low-energy photons.

The advantages of the perovskite-on-silicon cell have been described by Mártil in 2022 [11] who maintains that with the synergy of the two cells, it is possible to overcome the 30% efficiency barrier, [12] obtaining 'the best of both worlds.'

In July 2022, a new record in solar power generation was set when researchers at the Swiss Center for Electronics and Microtechnology (CSEM) and the École Polytechnique Fédérale de Lausanne (EPFL) achieved a power conversion efficiency exceeding 30% for a 1 cm^2 tandem perovskite-silicon solar cell. The breakthrough was confirmed by the US National Renewable Energy Laboratory (NREL).

Since the Lausanne lab breakthrough, researchers around the globe have concentrated their efforts on surmounting the 30% barrier. According to Stefaan De Wolf and Erkan Aydin in

2023, [13] tandem cells overcoming this threshold provided confidence that high-performance, low-cost PVs can be brought to the market.

Experts say perovskite-silicon tandems could theoretically reach efficiencies of around 45%. [7]

2.5 Planar Perovskite Cells and Transport Layers

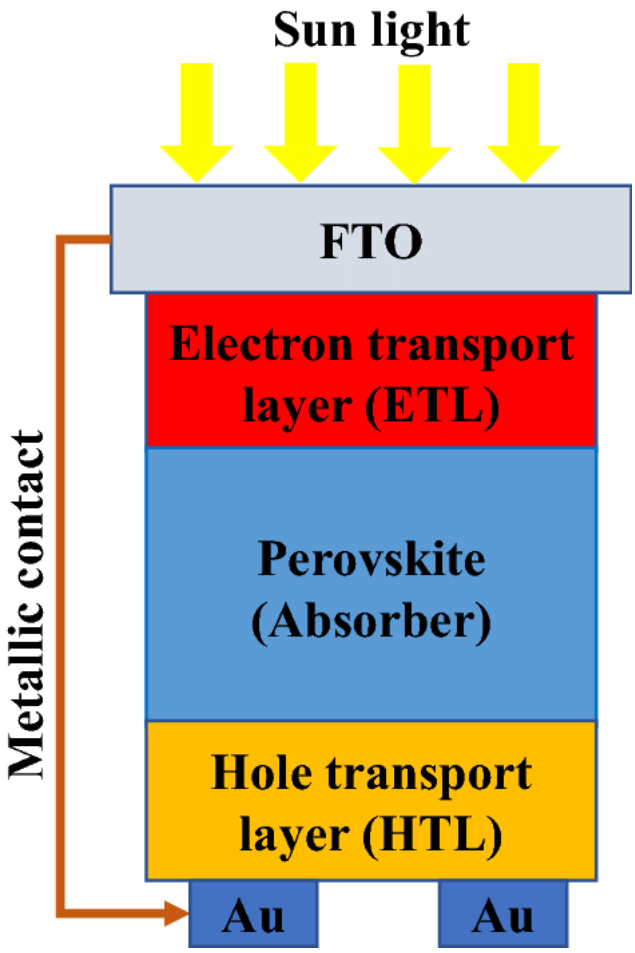

Figure 4 – Planar perovskite device structure

Over the past 10 years, single planar perovskite solar cells (PSCs) have achieved record efficiencies of 25.5% single junction solar cells (as at 2021) [*14*] and these efficiencies are rising impressively. This is in part due to their inherently low defect densities, tuneable bandgaps (making them perfect for tandem solar cells in conjunction with silicon-PV) and impressive optical and electronic properties.

The optimal perovskite band gap (i.e., wavelength that can be absorbed relative to that which the solar cell can efficiently utilize) is limited by the thickness of the perovskite material. Bag et al's results show that when a thin layer is used, low photocurrent results due to less absorption, however carrier extraction is high. In a thick perovskite layer, more carriers are generated in the device due to an increase in absorption but there is a lower collection efficiency due to recombination which affects V_{oc}. [15] Thicker materials also suffered increased parasitic energy absorption, an optical absorption process that does not generate an

electron/hole pair. This results in lost power, rather than the desired conversion of solar energy to electricity directly.

Perovskite solar cells can be completely solution processed using simple methods such as spin coating or slot die coating. This means that they may be compatible with roll-to-roll processing methods. However, constructing the highest performing PSCs requires highly optimized and controlled processing. So, these figures have not yet been achieved in commercial production environments.
These planar perovskite solar cells use several layers to effectively separate and extract charge. However, in its most basic terms, a planar PSC needs an absorbing perovskite layer sandwiched in between two charge transport layers (one to extract electrons and one to "extract holes").
It is therefore beneficial that the conduction band of the electron transport layer is lower than that of the perovskite. This allows the electron to passively diffuse away from the perovskite. In the hole transport layer, the energy level of the valance band should be close to or slightly higher than the perovskite's valance band so that electrons can quickly diffuse into the unoccupied "holes" in the perovskite before recombination occurs.

2.5.1 Charge Transport Layers

Choosing the best charge transport layers is extremely important when constructing an efficient perovskite solar cell. There are several factors to consider when making this decision, including processing limitations on substrates, band level alignments, device structure, wettability, and the chemical resistance of the layers.
Good charge transport layers extract charge efficiently, while decreasing recombination losses at the transport layer/perovskite interface which might lower V_{oc}.
Structurally, depending on whether the device has a regular or inverted architecture, the “bottom” transport layer must be smooth, uniform and have good wettability to ensure that a smooth perovskite layer can be deposited on top of it. This architecture is either a regular negative-intrinsic-positive or inverted positive-intrinsic-negative layer structure and refers to the mesoporous metal oxide layer sitting between the electron transport layer and the hole transport layer. [16]
Furthermore, the “illuminated” layers — through which light will need to pass to get to the perovskite absorber — must have good transparency to allow light through to the perovskite absorbing layer.

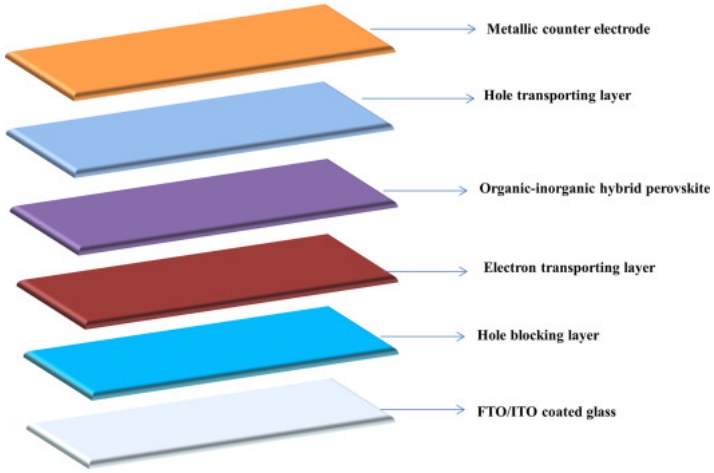

Figure 5 - Illustration of a typical perovskite solar cell structure. With the n-type compact layer, a mesoporous oxide layer, a light-harvesting perovskite layer, a hole-transporting layer and two electrodes [17]

2.5.2 Electron Transport Layers

Devices using a mesoporous TiO_2 layer were popular in the early iterations of PSCs devices due to their use in dye-sensitized solar cells. TiO_2 has reasonably good charge extraction properties and is also very chemically resistant so will not be affected by subsequent solvent processing. [18]

Both compact and mesoporous TiO_2 layers are still used in high efficiency PSCs. They are often used together where a compact TiO_2 layer ensures a full hole-blocking, electron-collecting layer while a mesoporous layer allows high levels of electron extraction. However, these layers can require high temperature sintering (>400 °C) and are very time consuming to produce. Additionally, TiO_2 has been shown to be vulnerable to UV light causing degradation of the perovskite layer, [*18*] which can sabotage device performance. SnO_2 has a wider bandgap than TiO_2 [*18*] and its band alignment makes it perfect for charge extraction with methylammonium-based ($MAPbI_3$) perovskites. Tin oxide also has high electron mobility in thin films and high chemical resistance and can be processed using a range of low-temperature methods, such as chemical bath deposition, spin coating, spray coating or slot die coating from nanoparticle suspensions.

In 2021, an SnO_2 ETL has been used to achieve the certified world record highest efficiency PSC of 25.5% at that time. Here, in combination with a chlorine-heavy perovskite precursor, a chlorine-doped SnO_2 interlayer was created between the SnO_2 ETL and perovskite layer,

increasing electron extraction. However, SnO_2 layers do often require annealing at 150 °C, which could be a problem for scale up when working with some polymer substrates. [17]

2.5.3 Hole Transport Layers

Spiro-OMeTAD is one of the most used hole-transport layers for PSCs. It regularly produces high efficiency PSCs — and is used in the current world champion device. [*19*]

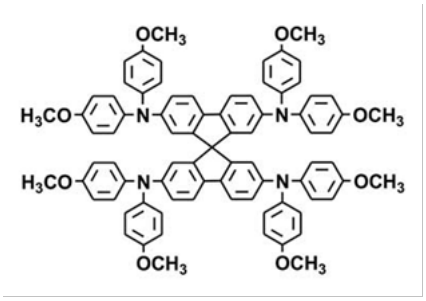

Figure 6 – Chemical structure of Spiro-OMeTAD

Spiro-OMeTAD can be purely solution processed and has no annealing step, meaning it can be processed easily at low temperatures. In fact, a Spiro-OMeTAD HTL has been shown to be compatible with large scale perovskite production, with Di Giacomo et al. *[20]* creating >15 cm^2 devices with over 10% PCE and Kim et al. [*21*] showing that devices using Spiro-OMeTAD created with completely roll-to-roll processes have a champion PCE of 13.8%.

However, Spiro-OMeTAD requires the addition of several dopants to achieve maximum conductivity, hole mobility and to ensure these dopants dissolve in chlorobenzene. Additionally, there is mounting evidence suggesting Spiro-OMeTAD may cause long term stability issues with PSC devices.

2.5.4 Energy Level Diagrams

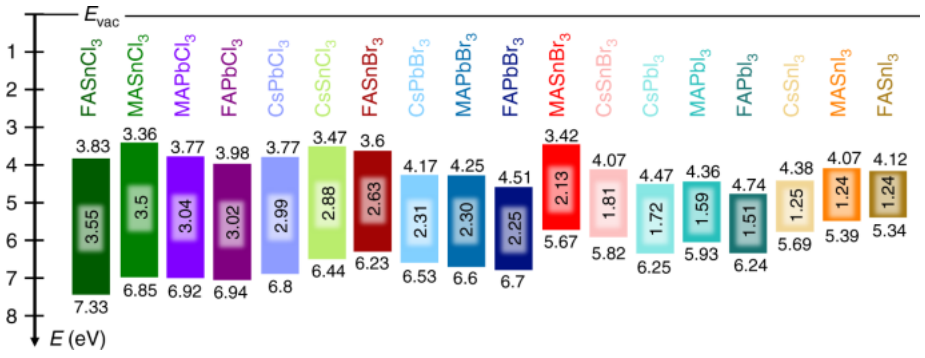

Figure 7 - Energy level diagram for perovskites and charge carrier materials used in perovskite solar cells [22]

Band level alignment is extremely important in perovskite solar cells. The figure above shows the band gap for several perovskites. When the perovskite absorber captures a photon, this results in both an electron in the conduction band (CB) and a "hole" in the valence band (VB). It is important to extract these charges from their respective layers as quickly as possible to avoid recombination. The HTL and ETL are designed to encourage the flow of electrons and holes across the interface with the perovskite absorber. SpiroOMeTAD is a common HTL and TiO_2 is a common ETL. [23]

The electron that is occupying a space in the perovskite's conduction band must be able to transfer easily into the conduction band of the electron transport layer. If the conduction band of a material is at a higher energy level than the perovskite's conduction band, however, there will be an energy barrier preventing this movement of electrons.

It is therefore beneficial for the conduction band of the electron transport layer to be lower than that of the perovskite. This allows the electron to passively diffuse away from the perovskite.

In the hole transport layer, the energy level of the valance band should be close to or slightly higher than the perovskite's valance band so that electrons can quickly diffuse into the unoccupied "holes" in the perovskite before recombination occurs. If the valence band of the perovskite is higher than the valence band of the HTL then electrons would not be excited out of this layer negating the effect of the incident energy. [23]

2.6 Different Perovskite Systems

Included here are recipes for making several different perovskite films and metrics of the solar cell devices made using these materials. All devices described here have the device stack:

ITO Coated Glass/SnO_2/perovskite/ Spiro-OMeTAD/Au

and these respective transport layers are deposited manually with a pipette. All perovskite layers and hole transport layers were deposited in a glove box environment which maintained a level of <0.5% relative humidity and <0.5% O_2. [18]

2.6.1 CsFAMAPb(I_xBr_{1-x})$_3$

Mixed halide *(Iodine, I, and Bromine, Br)* and mixed cation *(methylammonium, MA, formamidinium, FA and Cesium, Cs*) PSCs have consistently produced devices with relatively impressive stability and durability. Until the past few years, triple cation devices have produced world record PCE's. [24,25] Typically, these perovskites are processed in an inert environment to achieve the best performances, but nevertheless these perovskites are still extremely versatile. In 2020, Bishop et al. [26] demonstrated a fully sprayed PSC device using this high-performing triple cation perovskite (CsFAMAPb(I_xBr_{1-x})$_3$) of 1.2M with a 4:1 DMF/DMSO solvent blend ink, with small area efficiencies of 19.4%. This ink has been shown to be compatible with scalable techniques such as air-blading quenching. [27] However, there are some issues with triple cation perovskites. For instance, methylammonium is extremely volatile, thermally unstable and will degrade in the presence of oxygen or moisture. Therefore, its use in PSCs can significantly lower the lifetime of the device. However, when properly encapsulated, these PSCs have been shown to have great performance over several months.

2.6.2 $MAPbI_3$

Methylammonium lead iodide ($MAPbI_3$) is one of the earliest formulations of perovskite used in PSCs. Here Subbiah et al, dissolved 1.1M MAI with 1.1M of PbI_2 in DMF. This is typically a high performing perovskite and can be processed at relatively low temperatures. [28] Their primary use of methylammonium as an A-cation can lead to some intrinsic instabilities, so although they may have impressive performance initially, this may deteriorate over a matter of days, if not properly encapsulated.

As can be seen in Table 1, the average PCE over 3 devices of 6-pixels was 17.6 ± 1.1 % with the champion PCE for a single pixel of 19.3%, stabilizing at 18.4% over 1 minute. [29]

2.6.3 $CsFAPbI_3$

Due to the various instabilities of methylammonium-based perovskites, formamidinium base perovskites are an appealing choice when designing stable, high performing PSCs. $FAPbI_3$ also has a lower band gap than $MAPbI_3$, which means it can absorb a larger proportion of the sun's spectrum, leading to higher photocurrents and therefore better device efficiencies. [30]

However, $FAPbI_3$ is phase-unstable and requires high temperatures to convert fully to the black (α-) phase needed for perovskite solar cells, and to avoid falling into a less absorbing, non-perovskite (β-) phase.

There has recently been a surge of formamidinium-based perovskites which show impressive device stability without the use of methylammonium cations to stabilize the α-perovskite phase. As of Nov 2021, the certified highest performance perovskite device is a doped $FAPbI_3$-based perovskite achieving 25.5% PCE [*31*] and there have been several other extremely successful examples using $FAPbI_3$-based perovskites [*32, 33, 34*] including a slot die coated device with an active area of 20.77 cm^2 attaining PCEs of 16.6%. [*33*]

2.6.4 Comparison of these systems

Here is a table from Valadi et al comparing the PCEs of PSCs using the perovskites described in 2.6.1 to 2.6.3. [35]

Perovskite	**Average PCE (%)**	**Best PCE (%)**
Cs0.05FA0.81MA0.14Pb(IxBr1-x)	16.4±1.8	19
MAPbI3	17.6±1.1	19.3
CsFAPbI3	14.0±2.0	17

Table 1 - Example average and best PCE of perovskite devices [35]

2.7 Manufacturability

Scaling up perovskite manufacturing is required to enable commercial production of perovskite solar cells. Producing uniform, high-performance perovskite material in a large-scale manufacturing environment is difficult, and there is a substantial difference in small-area cell efficiency and large-area module efficiency. The future of perovskite manufacturing will depend on solving this challenge, which this research aims to progress.

Flexible perovskite solar cells can be lightweight, flexible and low cost which means they could be integrated into wearable mobile devices in the future. There is therefore increasing interest in the field of organic-inorganic hybrid perovskite solar cells. Recently the PCE (power conversion efficiency) of flexible perovskite solar cells has rocketed from the initial 6% to 18.4%. [36]

Many of the methods used to produce lab-scale perovskite devices are not easy to scale up, but there are significant efforts to apply scalable approaches to perovskite fabrication. Making the processes scalable and reproducible could increase manufacturing and allow perovskite PV modules to meet or exceed U.S. Department of Energy (DOE) Solar Energy Technologies Office (SETO)'s target for cost of electricity goals for PV.
For thin-film technologies, these can currently be split into two major production types:
Sheet-to-Sheet screen printing [*37*]: Device layers are deposited on a rigid base, which typically acts as the front surface of the completed solar module. This approach is commonly used in the cadmium telluride (CdTe) thin-film industry.
Roll-to-Roll [*38*]: Device layers are deposited on a flexible base, which can then be used as either an interior or exterior portion of the completed module. Researchers have tried this approach for other PV technologies, but roll-to-roll processing did not gain commercial traction because of the performance limitations of these technologies.
Another proven printing technology is ink-jet printing. This technology is cheap, and it has had widespread commercial and domestic use over many years. The technology has developed immensely and can be used to reproduce photographic quality images. This requires devices capable of precisely controlling the nozzles that create the size and production rate of the ink droplets. It has resulted in commercial printers that can achieve 5000 dpi at very low cost.
The use of ink-jet printing is proven in the fabrication of perovskite devices although to date this approach has not been used to deposit the perovskite. The carbon stack devices used in this research have been fabricated using screen printing methods and are therefore scalable. One advantage of inkjet printing is that no mask is required as the inkjet can be programmed to deposit on a certain active area. This eliminates both stages in the manufacturing process and also waste of materials thereby streamlining it on two fronts.
Another advantage is that it's an ideal method when dealing with a rigid substrate which are still largely required for the carbon stack as the high temperature annealing required in production is in excess of 400°C and limits the flexible substrates suitable for use, such as PET.

Previous work with the carbon stack has focused more on using the inkjet printing technology to replace the screen-printing method currently widely used. This therefore means

that much of the literature deals with inkjet printing the layers of the carbon stack such as the TiO2 layer rather than working with perovskites.

Another established advantage of the mesoporous carbon perovskite solar cell over other structures is that the triple layer structure can be manufactured but not infiltrated and the stacks can be stored. The perovskite can then be infiltrated as needed to produce devices on demand. This approach was adopted during this research project with batches of cells made and stored ready for the hard temperature annealing and infiltration using the inkjet printer to be carried out as part of testing.

Inkjet printed carbon stack solar cells were assessed by Verma et al. [39] with four of the 5 layers being inkjet printed, just not the perovskite precursor. It was possible to produce "large area solar cell devices with an efficiency of 9.1%". The perovskite was then pipetted onto the stack. The MAPI ink was infiltrated into reference monolithic stacks which achieved a power conversion efficiency of 13.5%. This was a breakthrough for a device area larger than $1cm^2$.

Semiautomatic pipetting, through the use of an Eppendorf pipette, has the disadvantage of liquid thickness variations with a larger volume of liquid being found in the centre of the device. Despite the aspiration and deposition of the perovskite solution being controlled, a single pipette is still held over the centre of the active area for the deposition process. This leads to deterioration of the upper layers of the carbon electrode. At low filling volumes, the cells turned yellow and after three months of exposure to ambient atmosphere, which revealed the transformation of perovskite into PbI_2. However, fully infiltrated stacks remained black, indicating the formation of a passivation layer protecting the active perovskite material underneath. [40] The key is to optimise the deposition of the perovskite so that the stability of the cells was increased.

The current method of screen printing produces cells of good efficiency, but compromises on the lifetime of the cells as they begin to degrade. Perovskite solar cells with mesoporous TiO_2 electron transport layers have previously reached >22% efficiency at the laboratory scale ($<1cm^2$) usually fabricated using spin coating. Such cells have been reported to last >10,000h without notable performance losses.[40]

Inkjet deposition of the perovskite layer prevents this degradation as precise volumes of ink can be deposited. In the case of the paper by Aron J. Huckaba et al. [40] they concluded

inkjet deposition of the perovskite and also the TiO_2 two layer, could contribute to longer lifetimes of carbon mesoscopic perovskite solar cells.

Using inkjet deposition power conversion efficiencies of 8.5% for an active area of 0.16cm^2 for MPSC have been reported by Hashmi et al [41] using these carbon stack devices with high spatial resolution.

Inkjet allows for this stage of production (perovskite deposition) to be integrated into a production line (possibly roll-to-roll) on a larger scale. Particularly as the inkjet can be used over large areas which is not the case with spin coating. Inkjet printing is a digital, mask-less and contact-less fabrication technique and allows full pattern control, where the pattern resolution is only limited by the droplet volume and the spreading diameter of the droplet on the substrate. [42]

In piezoelectric drop on-demand (DOD) inkjet printing droplets are ejected by a pressure pulse generated in a fluid filled cavity by a piezoelectric actuator. This technology employs 100s of individually addressable nozzles with jetting frequencies in the kHz range. This allows for very precise deposition of the inks and the possibility of multiple printing passes. This is further encouraging in terms of pursuing this technology when working with the carbon stack.

For this project the SUSS LP50 desktop R&D inkjet printer was used with PiXDRO technology. [42] The Spectra SE 128 printhead was used for the full range of tests and prints conducted as part of this body of research. The Spectra head had 128 nozzles formed of 64 addressable channels set on two independent piezoelectric slices.
This printer was used in other research [43] although many other papers used different printheads with fewer nozzles such as the DMC printhead.

The idea that it is challenging to inkjet print nanoparticle inks due to nozzle clogging is already established. However, there are also many advantages to this method of production using the perovskite inks and there is now increased interest in inkjet as a method of manufacturing cells due to the success of lead halide perovskite solar cell PSC technology.

Drop on demand inkjet can be used for the fabrication of monolithic mesoscopic carbon-based perovskite solar cells – by printing all layers of the stack as well as the active perovskite layer. As shown by the work done by Anand Verma et al [39] which also compared inkjet printed cells to traditionally manufactured screen-printed cells. This research also provided insight into the challenges faced when applying this technique to perovskite, namely the clogging of the nozzles due to printing with the nanoparticle perovskite inks.

The use of the inkjet printing method of deposition reduces the "human error" aspect of production [39] that spray methods of deposition currently have. This automation of the deposition process could lead to a higher probability of device performance and reproducibility making it easier to produce larger batches of cells with similar PCEs. This is another positive attribute of the application of this technology to the production process of the carbon stack perovskite solar cells as it further aids the scale up effort.

Another advantage of this technology is that the inks can be used to print the cells in ambient conditions. This means that auxiliary costs such as heating the working environment do not have to be considered when examining this method and its potential at a larger scale.

The cells made using the inkjet tech [39] were compared to screen printed cells which provided an interesting comparison. In this paper the cells had an area of 1.5cm2 and a performance of 9.1% which is high enough that this could be seen as a viable method of production worth developing as the inkjet technology could be easily scaled up. Whilst this was not directly possible during this project, the idea of comparing the standard deposition method for larger scale single cells using automated pipette with the inkjet printer was established.

Verma's work has achieved both the sequential deposition of thin m-TiO2 and the perovskite layer to achieve an average efficiency of 12.2% on small laboratory cell areas. [39] Infiltration of methyl ammonium lead tri-iodide ($MAPbI_3$) perovskite precursor was carried out on the MPSC – carbon stack. It was infiltrated with the standard MAPI by inkjet at room temperature. The cells were characterised and compared to standard screen-printed devices. The advantages of precise, waste-free infiltration using inkjet are highlighted and guide printing speeds are provided. [39]

2.8 Inkjet Printing inks

Non-halogenated solvents are also researched and trialed as part of this research. Previous work had proven that the inkjet printing could be used to create the substrate layers and demonstrated that waste free infiltration could be achieved by using inkjet deposition.

Much research exists into the correct composition of the inks which shows optimised ink composition consists of three important parts: high viscosity solvent, low viscosity solvent and humectant, which is important to minimise evaporation and clogging at the nozzle. Viscosity, surface tension and density of the ink are all important, while the vapour pressure also influences the drying time and final quality of the film.

In further work by Aaron J Huckaba et al solvents with a low vapour pressure and high polarity to create a uniform layer of nanoparticles with minimal particle migration were reviewed. [40]

The first cells fabricated focused on how device performance was affected by drop spacing (this was done using a single pass). Two interrelated factors affect film thickness, these were drop spacing and the number of layers deposited (this is when the concentration of the of solid material is kept constant).

Drop spacing is defined as the distance between the centre of two adjacent droplets on the substrate. At low drop spacing values (e.g. 10μm), Huckaba et al found the nanoparticles in each droplet exhibited large overlap, while at high drop spacing values (e.g. 100μm), there was little to no overlap. Smaller droplet spacing means more droplets are printed (higher dpi) to cover the desired print area than with larger droplet spacing, which also translates to thicker films. Huckaba et al noted that "Drop spacing values are highly ink and substrate specific and rely on parameters such as the surface free energy of the substrate surface, substrate surface roughness and surface tension of the ink."

For single pass printing the thickness can be increased by reducing drop spacing therefore increasing dpi and the amount of ink deposited on the substrate. More ink deposition can also be achieved by increasing the number of passes of the printer.

Huckaba et al found that the prevalence of pin-holes increases with increasing drop spacing, due to the decreasing amount of ink present and the distance between each printed droplet. When used to print TiO_2 no larger differences in morphology were observed between drop spacings of 20 and 35μm. [40] At a drop spacing of 50μm poor film homogeneity was recorded. The thickness of the TiO_2 substrate linearly increases with the number of passes of the printer. Fill factor, short circuit current, open circuit voltage – were all recorded for a number of drop spacings.

Then the performance of cells with an increasing number of passes was examined. This ranged between 1 and 6 passes. In general, it was found that adding layers lowered the device short circuit current values and the fill factor values. [40] This research also looked at how substrate temperature affected the print and performance of the solar cell. At a higher substrate temperature, the evaporation rate at the centre of the deposited droplet forced an enhanced Marangoni effect from the droplet edges to the centre. Top view SEM was used to analyse morphology and to measure the thickness of the deposited films. With a strong Marangoni flow, Huckaba found the coffee ring effect was found to be reduced, and the surface coverage of nanoparticles can be thought to exhibit a convex surface morphology instead of the concave surface morphology that comes with an enhanced coffee ring effect.

This work also provided guidance on the sensitivities of the parameters of deposition to the environmental conditions and how these could be optimised. The morphology of the printed film was characterised "Inkjet deposited mesoporous films for $MAPbI_3$ absorber layers, enhances the device performance due to enhancement of J_{sc} and FF values when substrate temperature is 60degC during deposition" Overall, there was an improvement in performance when compared to spin coated cells.

Hashmi et al worked on the inkjet infiltration of the perovskite precursor ink and the stability of the cells that use this method of infiltration. [41] It was "performed over the triple layer (TiO2/ZrO2/C) porous stack with Fujifilm's Dimatix inkjet printer (Model DMP – 2831)" The precursor ink contained 5-AVAI (5-ammonium valeric acid).

A stable precursor ink is required to overcome issues such as fast crystal formation within the perovskite and therefore clogging of the nozzles leading to an inconsistent print process.

This stable precursor ink works to produce precise infiltration and printing of the perovskite absorber layer whilst not damaging the print head of the printer cartridge.

Hashmi et al observed very high stability of perovskite precursor ink which was formulated by mixing the PbI2 and MAI with the 5-AVAI. This ink has been used as a templating agent to improve the crystalline network and charge carrier lifetime of the $CH_3NH_3PbI_3$. The 5-AVAI also significantly slows down the perovskite crystal growth therefore preventing the inkjet printer cartridge from clogging – it provides an opportunity for precise patterning and controlled volume dispensing of precursor ink.

Precise dispensing of known volumes of the perovskite precursor ink tunes the photovoltaic performance of carbon-based PSCs. 10cmx10cm FTO-glass substrates having 18 individual cells were used for testing. They were measured in the solar simulator to analyse the photovoltaic performance. The thickness of the ZrO2 in Batch 1 was also varied by increasing the number of layers printed (1-4). The combined thickness of the TiO2 and ZrO2 were measured with a profilometer and varied between 1.7-2.9μm. The volume of perovskite deposited was also altered for this batch to 3.18μL which was enough to saturate the triple layer stack with combined TiO2 and ZrO2 thickness of 2.3μm. However, this volume of fluid was not enough to saturate the cell with combined TiO2 and ZrO2 thickness of 2.9μm although the performance of these thickest cells was still almost as good as the cells measuring 2.3μm combined thickness. For the thickest cells Hashmi et al increased the volume of ink to 3.71μL which resulted in a significant boost to the J_{sc} and efficiency of the cells.

An additional batch of cells was subjected to continuous one sun illumination at 35degC over a period of 1046 hours without any encapsulation. This testing revealed exceptionally high stability with almost no change in overall efficiency. Nevertheless, there were some mild signs of degradation – yellowing in some devices which could indicate formation of lead iodide. The age cells were found lighter than the fresh ones. Although changes were not visible to the human eye.

The possible change in CH3NH3PbI3 absorber material between fresh and aged cells was analysed through XRD. There is no feature of PbI2 in the XRD pattern of a fresh device but

there is a negligible feature in the age devices corresponding to the PbI2 phase confirming very slight degradation of the cells.

Hashmi et al [41] concluded that automated and precise inkjet infiltration of perovskite precursor remarkably improved the performance reproducibility among the fabricated devices. This reliable process control is considered key to larger scale production of any device.

Hashmi also tested the stability of the cells in dark storage. [41] Storing them in the dark for three weeks there was a remarkable enhancement in the overall efficiency of the cells (=13%) there was a noticeable improvement in fill factor. The improvements in the performance were considered as a result of the further curing of the perovskite absorbing layer in vacuum which provided additional time to improve its crystal growth.

The capability and potential of inkjet infiltration of highly stable perovskite precursor ink for porous triple layered HTM free printed PSCs was successfully demonstrated by Hashmi et al. [39] The automated inkjet infiltration allows homogeneous dispensing and distribution of perovskite precursor ink on the active electrode area, which provides a high probability of device performance reproducibility and a reduction in "human error" that spray methods could have.

2.9 'Green' Solvents

There are legal restrictions placed on the procurement and use of γ-butyrolactone (GBL) that limit its viability when looking at scaled-up levels of production. This is due to its toxicity and conversion in the body to GHB making it a heavily controlled substance. GHB and GBL are both Class B drugs in the UK - but GBL is available for legitimate use in industry. Since 2021 the exemption for industrial users has been revoked and industrial users of GBL now require a controlled drugs licence. [44]
γ-valerolactone (GVL) can be used as a nontoxic, biodegradable, green alternative to GBL for carbon stack perovskite solar cell fabrication [45] making it a viable replacement, and potentially more attractive, option when considering the scale-up of perovskite solar cells.

The two solvents have similar chemical structures as shown by the figures below (figures 8 and 9).

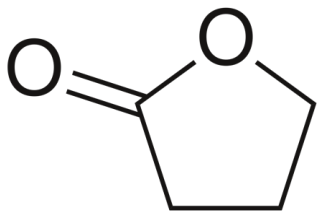

Figure 8 – Chemical structure of GBL

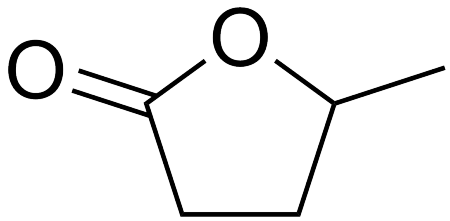

Figure 9 – Chemical structure of GVL

In summary, the exploration of green inks for inkjet printing in triple mesoscopic perovskite cells offers a real opportunity to overcome the barriers to scale up to commercial production utilising perovskite technology.

3.0 Experimental Procedure

All experiments were carried out in the SPECIFIC laboratories in Engineering faculty using calibrated equipment, for example the rheometer, calibrated using water as a baseline reading due to known viscosity, and all necessary personal protection equipment.
The hazardous nature of the materials used in the creation of the cells required an understanding of, and strict adherence to, the rules and procedures governing the handling of these substances throughout the project. Additionally, as the practical research aspect of this project was undertaken during 2020 and 2021, all prevailing Covid-19 pandemic regulations were observed.

The experimental work comprised:

- Manufacture of the mesoporous carbon stacks
- Manufacture of the perovskite inks
- Use of rheometer
- Use of Pixdro LP50 inkjet printer in analysis and deposition of the inks
- Use of a solar simulator and collection of data

3.1 Manufacture of the mesoporous carbon stack

Materials Used:
Titanium diisopropoxide bis (acetylacetonate) (TAA, 75% in IPA, Sigma-Aldrich), anhydrous 2-propanol (IPA, 99.5%, Sigma Aldrich), TiO_2 paste (30NR-D, GreatCell Solar), ZrO_2 paste (GreatCell Solar), Carbon paste (Gwent electronic materials) and terpineol (95%, Sigma-Aldrich) were used as received. Precursor materials: PbI_2 (99%, Sigma-Aldrich), MAI (CH_3NH_3I, anhydrous, Dyesol), 5-ammonium valeric acid iodide (5-AVAI, Dyesol), γ-valerolactone (GVL, Sigma Aldrich)

Process:
The glass substrate was cleaned using a highly alkaline soap (Helmanax) to ensure there was no dust or grease present. Both sides of the glass were scrubbed with a diluted solution of the alkaline soap. The glass was rinsed using distilled water and dried using the N_2 ‘gun’. Acetone and then IPA (isopropanol) solutions were poured over the glass. The acetone was

used first to lift any streaks of grease from the surface, and these were then washed off by the IPA solution. Finally, the substrate was plasma cleaned for 5 minutes.
After preparation, the glass substrate was treated with a blocking layer of C-TiO_2 (compact titanium oxide) diluted in IPA which was applied manually using a spray gun.
The glass was sprayed 25 times (by 14 passes there should be a visible iridescent film on the foil. At 25 passes the remaining C-TiO_2 IPA solution was measured, if not enough had been used additional passes over the substrate were made.)

A pattern was followed to ensure even coverage of the whole substrate area. Each pass took 4 seconds across the substrate area, and 5 passes were made down the substrate starting at different corners each time to ensure all areas had similar coverage.
The glass substrate was placed on a hot plate at 300°C for the spraying process.

The three mesoporous layers making up the complete carbon stack, were then screen printed onto the glass substrate, these are:

Layer 1: TiO_2 – mesoporous electron transport layer (ETL)
Layer 2: ZrO_2 – mesoporous insulating layer
Layer 3: Carbon top contact – porous conductive layer

The three layers were screen printed onto the glass substrate. This process was carried out in an ISO 6 cleanroom to prevent particle contamination of the printed layers. After printing each layer, the mesh was cleaned using IPA in a fume cupboard.
The mesoporous stack was then annealed at 400°C for 20 mins to remove the organic binders and prepare the stack for the infiltration of the perovskite ink.

3.2 Manufacture of perovskite inks in the glove box

The perovskite ink solution consisted of PbI_2, methylammonium iodide (MAI) and ammonium valeric acid iodide (AVAI), a cation additive, were dissolved in GBL. The GBL was substituted for GVL later in the project.

For this project the most common volumes of solution made were 5mL or 10mL solutions.

The preparation of these solutions was carried out in the glove box in the clean room. This was to ensure both a lack of contamination of the solutions and a safe working environment. The MAI was weighed out first, then the AVAI and finally, the PbI_2.

For one mL of solution:

506.2mg PbI_2

175.3mg methylammonium iodide (MAI)

7.8-8.6mg AVAI

These were all in powder form and were then dissolved in either 1mL of GBL or GVL solvent depending on the solvent system being worked with.

Glove box usage:

The preparation of the solution took place in the glove box within the Cleanroom laboratory. This was to comply with safety standards set for handling of the lead iodide in powder form. The required materials were placed in the glove box using the antechamber and vacuum system.

The MAI was weighed out first followed by the AVAI and finally the PbI_2.

For the MAI and the PbI_2 a metal spatula was used. For the AVAI an antistatic spatula was used due to the nature of the powder.

A 1 mL Eppendorf pipette was then used to measure out and add the required volume of GBL (later GVL) to the solution.

On completion of the solution the powders and GBL were returned to their storage within the glove box.

The waste bag and solution were retrieved from the glove box and the waste bag disposed of in the hazardous waste bin (pipette tip into sharps).

When the GBL is used for the perovskite ink, the solution must be left on the hot plate at 70°C until fully dissolved. When GVL is used in the solution, it does not need to be heated but does need to be left on a mixing plate.

3.3 Rheometry

The measurements were taken at an ambient temperature of approximately 18°C (this was noted with each measurement to ensure that temperature did not influence the viscosity

results) using a Rheosense microvisc with an internal chip with 400-600cP sensitivity range. 10-12 measurements were made for each of the samples and a mean value was taken. All measurements were obtained using the 'auto-mode' programme on the rheometer. Shear stress was set at an automatic value of 2000N/m^2 with the auto mode measurement.

Prior to carrying out the main body of work the rheometer was calibrated using a distilled water reading returning a viscosity value of 1g/cm^3 and confirming the readiness of the machine. After the calibration of the machine had been checked the pipette was filled with the solvent used as the base for the ink solution – either GBL or GVL.

A cleaning program was then run fully depressing the pipette and pushing all of the liquid through the measurement chamber. This ensured that the result would be more accurate when measuring the ink solution. A reading was also taken with the solvent so that a base reading for a clean system was established, enabling confirmation that any following results for the different concentrations of the perovskite solutions were accurate. This solvent reading was taken at the beginning of every measuring session and compared with previous results.

To take the required viscosity measurements the pipette was filled from a 5mL vial of the perovskite solution and then inserted into the rheometer. The higher the viscosity of the solution being measured, the less of the solution was pushed through the measurement chamber to collect a reading. For higher viscosity concentrations of the solution this allowed for multiple readings to be taken with one pipette of solution.

To ensure that the nanoparticles in the solution had not fallen out of suspension and clogged the measuring chamber of the rheometer; after the measurements had been taken for the perovskite solution, a cleaning program was run with a full pipette of GBL solvent. This was to ensure any remaining particles of the perovskite were flushed through the system and removed to the waste container. After doing this twice, the system was then flushed through with a pipette full of distilled water. A test was conducted with this pipette to check the viscosity level had fallen back to 1g/cm^3 indicating that the system was clean and only water was being measured. If the measurement was not 1g/cm^3 when the water was tested, the cleaning program was run again with the solvent to ensure any remaining residue was removed from the system.

A pipette filled with air was then inserted into the system and the cleaning program was run to remove any remaining liquid at the end of a measuring session. The waste container was removed after all measurements and cleaning had been conducted and the waste solution was disposed of into the halogenated waste disposal Winchester. IPA was then used to ensure any perovskite particles were removed from the waste container.

3.4 Set-up of the inkjet printer

The SUSS LP50 printer was used for this project. The system was used with an aspiration system due to the presence of lead within the perovskite solution and also due to working with GBL.

3.4.1 Switch on process

The PixDro PC was powered up and the aspiration system turned on and the printer hood opened.
The print head used for the session was placed in the machine making sure to line the magnets up, so it was secure. The wires from the back of the print head were connected to the ink chamber.
The ink levels in the ink waste jar were checked and, if over 100ml, were emptied into a halogenated waste Winchester.
The printer was then switched on.
The ink chamber was filled with ethanol (or alternative suitable solvent), keeping the ink back pressure low to avoid bubbling (this was approx. -10mPa for ethanol)
The system was purged repeatedly to flush the ethanol through the system. This was to get rid of any air and make sure the system/print head was clean.
A suction was also sometimes required (found in maintenance menu) to make sure the print head was as clean as possible.
The nozzles were then inspected by going to drop view on the PixDro programme, and opening the head, to check to see if any droplets were falling.
The droplets were not particularly uniform with ethanol, but it could be seen if the nozzles were jetting. If there were no droplets falling the purge was repeated, the printhead cleaned (with paper towel) until droplets of solvent could be seen.

3.4.2 Notes on operation

There are various printing programmes, called recipes, that could be run. The Spectra Signature V2 was a good programme to run to see how many nozzles of the 128 on the Spectra head were printing successfully.

Increasing the QF (Quality Factor) of a recipe can improve the print quality, as multiple different nozzles are used to print one section. The QF can be increased as high as the number of nozzles being used for the print. For example, if 20 nozzles are active the highest QF will be QF20. It decreases the likelihood of large sections of the deposition area having misprints, as the higher QF also increases the variation in nozzle usage rather than having one nozzle repeatedly printing for a whole section of the print. This means that if there is a clogging issue with this nozzle, it will not affect the deposition as much if it is only used one in 20 times rather than for example one in two times.

Advanced drop analysis (ADA) is a tool used to find the optimal parameters for a print – it also opens up the 'custom' window along the bottom of the screen which can be used to further alter parameters. This can be accessed by selecting the required ADA recipe (in the recipes section) for the print head being used. This is a useful tool when determining the optimal parameters for deposition of the correct amount of perovskite or other ink onto the carbon stack/substrate.

The parameters of the piezoelectric wave and their effect on the behaviour of the ink were explored using the advanced drop analysis programme.

The parameters that could be adjusted on the inkjet printer as part of the ADA were:

- Peak time of the wave
- Rising edge of the wave
- Falling edge of the wave
- Voltage of the wave

The temperature of both the print head and the print table could also be controlled in the programme. The print head was always set to 20°C so that the RT value was always constant, but this could be changed for optimal operating. The normal temperature setting for the table was 30°C. Changing the temperature of the table affected the drying speed of the ink used, so

this parameter could be used to alter the behaviour of the ink. The maximum possible temperature was 90°C.

It was important to keep the head in the service position with the head off whenever changing any of the controls, preparing programmes or setting a start position for printing. This raised and therefore protected the head and also meant ink did not drip onto the table/rest of the machine as the head was prepared for printing.

Cleanliness is key to getting a good print and so ideally the machine was left on a cleaning programme overnight before attempting to print the next day. This optimized the number of nozzles that were working when it came to printing. When using perovskite this also lowers the health risk as less manual cleaning is required.

The ink back pressure (found in controls) must be as high as possible without causing bubbles to appear in the ink chamber. For a good ink this should be approx. -20mPa. This kept the ink droplets suspended so precise droplets fell from the head rather than a stream of ink.

'Drop view' was used to change the firing frequency of the droplets (also the LED parse speed). Drop view is a useful tool when setting up a print. It is this section that was used to optimise the wave pulse shape so that the maximum number of nozzles were operational. See figure 10.

Pulse shape A = even numbered nozzles
Pulse shape B = odd numbered nozzles

Opening the cover/hood of the printer cancelled any errors present in the system.

To print when the parameters have been optimized in drop view go to the print view screen. A starting position for the print was set using the jog feature to move the head and the table to the desired position with no offsets. (Some print programs will have an offset built into them).

It was also useful to do both a print and a simulation when printing to see a detailed picture of which nozzles were used in which area of the print in the simulation.

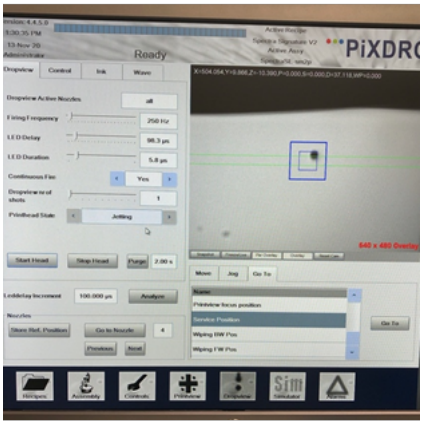

Figure 10– An example of the computer screen showing the 'dropview' tab in the PixDro software

The drop view was facilitated by a camera set up below the print head so that when in the ADA position the droplets could be viewed falling from the printhead.

3.4.3 Post print cleaning

After printing and emptying the ink chamber, it was filled with ethanol (or alternative suitable solvent), keeping the ink back pressure low to avoid getting bubbles.
In the service position the print head was set to start jetting to begin cleaning. The system was purged repeatedly to flush the ethanol through. This removed any residual ink and made sure the system/print head was clean.
When this cleaning process was completed, and the chamber was empty of solvent the inkjet was switched off.

3.4.4 Switch off process

This was the reverse of the switch on process. The print head was placed in the service position, then the controls turned off - Head voltage, temperature, ink back pressure etc. making sure that HBP power was turned off last.
The printhead was disconnected and removed. The printhead was then thoroughly cleaned and then put away.

3.5 Printing using the inkjet printer

The Spectra head was used for all deposition done in this project. This head was chosen because the 128 nozzles would maximise print speed therefore minimising the time taken per print. This choice also aimed to make the process as efficient as possible, maximising the number of nozzles open at any one time despite clogging.
The 'recipes' section of the inkjet contained various programmes you can run that will create different print patterns.
For set up and testing of the nozzles the 'spectra signature V2' is a good program to use as it uses each of the 128 nozzles in the spectra head to print the corresponding number onto the substrate, therefore making it easy to see which nozzles have blockages.

3.6 Post printing treatments

One area of post printing treatment that was addressed during testing was the 10-minute rest time at room temperature that cells underwent before being placed on the hot plate.
Due to the inkjet printer having a base plate/printing deck that could be heated, tests were run to see if the prints could be carried out at the temperature specified for the hot plate curing treatment, to further streamline the production time for the cells. However, eliminating this 10-minute rest time at room temperature led to the perovskite drying too quickly and therefore limiting infiltration of the precursor through the carbon stack. This resulted in reduced efficiency in the cells produced using this method, so the 10-minute rest time was reinstated.
Further to this work, tests were subsequently done increasing the rest time of the cells post print to 15 minutes. This extended rest time led to the highest percentage of infiltration in the cells and therefore to the highest efficiency values recorded as part of testing carried out on the solar simulator.

3.7 Preparation of cells for solar simulator testing

After the print run had finished for each cell, it was removed from the inkjet base plate and placed into the adjacent fume hood for a period of fifteen minutes to allow initial crystallisation to occur at room temperature.

The cell was then placed on a hot plate held at 45°C in the low humidity room for a period of one hour to complete the drying and crystallising process. After which it was removed and placed in a low humidity oven overnight.
The contacts for the cells were then soldered – using silver solder with an ultrasonic soldering iron – the results of this step can be seen in Figure 11.
The cells were then ready to be examined using the solar simulator.

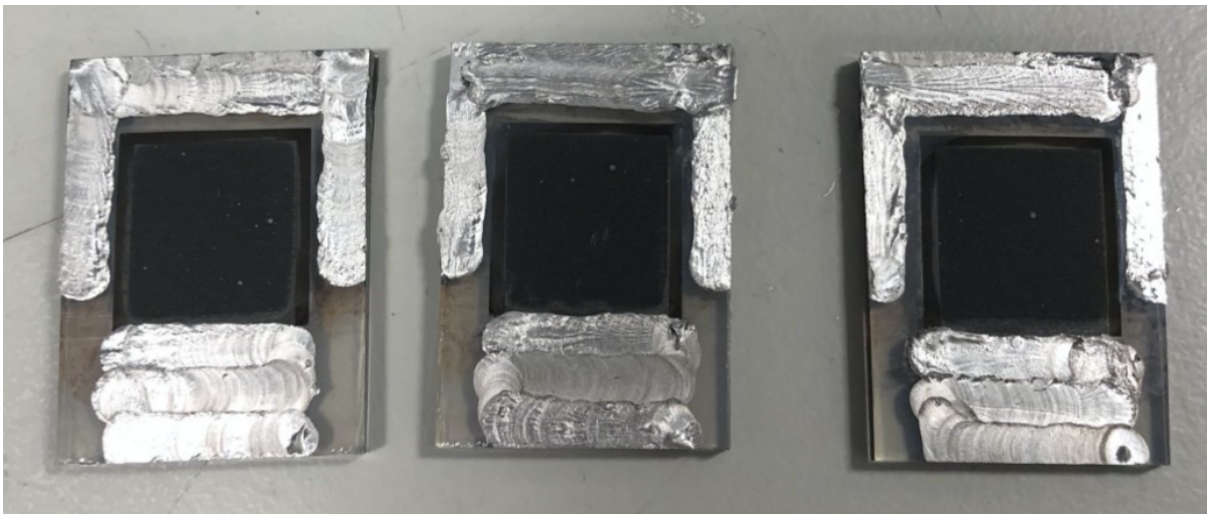

Figure 11 – infiltrated carbon stack cells, ready for solar simulator testing

3.8 Solar Simulator testing

To measure the efficiency of the cells a current-voltage measurement (J-V measurement) was taken using a Keithley 2400 source meter and class AAA solar simulator (Newport Oriel Sol3A) at 1 sun illumination. (These were calibrated against a KG5 filtered silicon reference cell, Newport Oriel 91150-KG5.) The devices were light soaked for 180s and then scanned at a rate of 100 mVs -1 from -0.2 - 1.1 V and then vice-versa. This was necessary to account for the well characterised slow response of devices using AVA.

4.0 Results & Discussion

4.1 Introduction

The literature highlights the importance of using a suitable ink for the deposition method chosen, as this significantly impacts the performance of the finished cell.

As such, initial work done on this project focussed on the analysis of the perovskite ink that would be used in the inkjet deposition process. This involved working with various increasing concentrations between 0.6 ml and 1.2 ml of perovskite precursor to ascertain the maximum concentration that could be infiltrated using the inkjet, while maintaining the stability of the solution. Thereby aiming to make the cells produced as efficient as possible.

The second stage of analysis of the perovskite ‘inks’ involved testing and comparing the performance of two different ‘green solvents’ used for the solutions. The two solvent systems were GBL MAPI and GVL MAPI. Testing was carried out to ascertain the optimum parameters for use of these solvent systems in the inkjet printer. Additionally, the properties and behaviour of the inks when being deposited were compared. This then informed the work done in the final stage of testing where the ‘inks’ were infiltrated into the carbon stack and the resulting cells were tested using the solar simulator.

The initial stage of testing was the rheometer analysis.

4.2 Rheometry

The rheometer was used to determine the viscosity of various concentrations of GBL MAPI and GVL MAPI and their suitability for inkjet deposition. The ideal viscosity range for inkjet printing is between 1 and 20mPas as stated by Li et al. [19]

The first tests conducted on the rheometer concerned the GBL and GVL solvents with no perovskite. This was done to provide a direct comparison between the two solvents outside of a solution. The two solvents were found to be of similar viscosities, but GVL was found to be marginally more viscous when tested using the standard programme of the rheometer (as shown by Fig. 13).

After ascertaining the behaviour of the solvents in isolation, testing was carried out on both the GBL MAPI and GVL MAPI systems.

The rheology tests carried out on various concentrations of the perovskite solutions also followed the trend of the GVL having a marginally higher viscosity, as shown by the direct comparison between the GBL MAPI at 0.95mPa.s and the GVL MAPI at the same concentration. (Fig. 12) The solution using the GVL was found to have a higher viscosity of 6.43mPa.s.

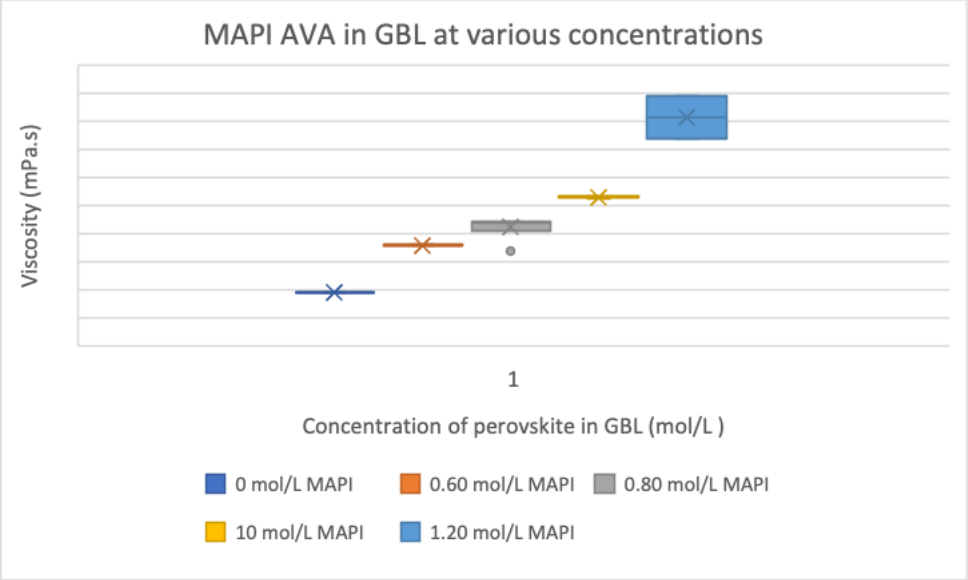

Figure 12 – Results of rheometer testing of various concentrations of MAPI AVA in GBL solvent

A box plot graph was plotted to illustrate the results of the viscosity testing. As shown in figure 12 the results correlated very strongly therefore were also plotted as averaged values as shown in figure 13.

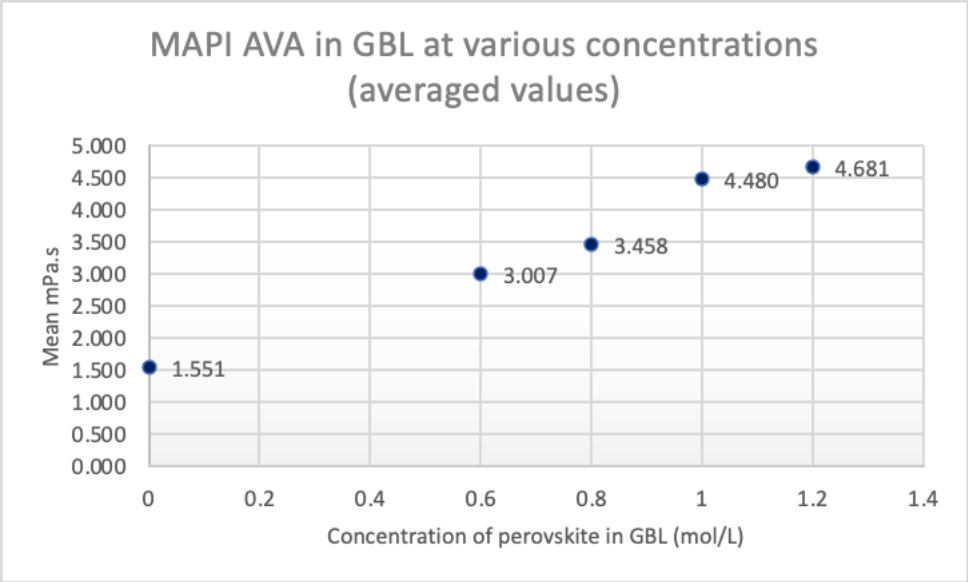

Figure 13 – Averaged results of rheometer testing of various concentrations of MAPI AVA in GBL solvent

When working with the GBL based solutions the concentration of the perovskite solution was increased by 0.2mol/L each test to determine the highest functional concentration of the solution that could potentially be used for printing. The final solution tested with the high concentration value of 1.2mol/L led to the solution precipitating when measuring and caused difficulties with the filter of the rheometer. This led to the conclusion that the solution was too unstable to progress to the next phase of testing and that the same issue would occur when using this solution in the inkjet printer, so higher concentrations were not attempted. The other reason higher concentrations were not attempted was due to the fact that at concentrations higher than 1.2 mol/L the solution crashes generally, meaning that it would not be stable enough to use as an ink for the inkjet process.

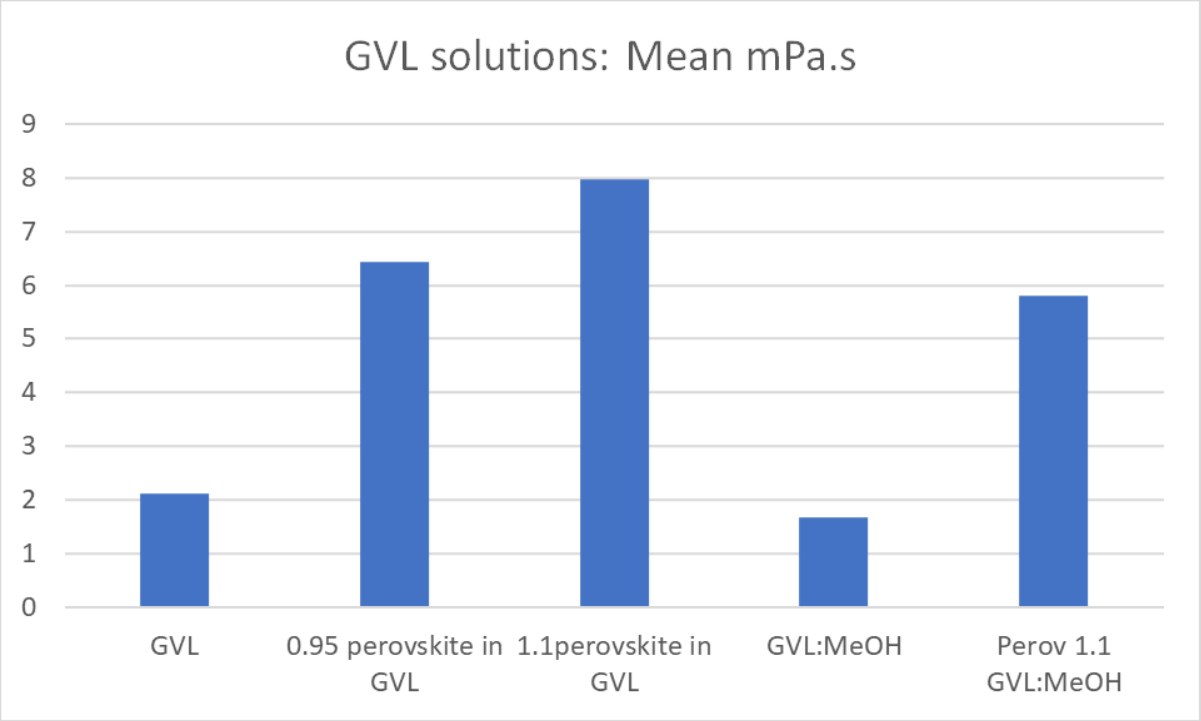

Figure 14 – Comparison of viscosity of different GVL systems

Figure 14 shows the viscosity of GVL systems an includes results from earlier work carried out by Carys Worsley. The comparison between the GVL and the GVL MeOH was an additional test to examine the properties of these two systems as part of her work on the green solvents.

The MeOH solution was not pursued further as an option for deposition via inkjet printing as the viscosity was lower than the GVL system. Once the first ADA and deposition tests had been run on the inkjet printer and the better results were achieved with inks of higher viscosity the MeOH option was set aside.

4.3 Advanced drop analysis (ADA) – GBL MAPI optimisation

The second, and most comprehensive, stage of research into the suitability of the perovskite solutions for inkjet printing involved utilising the inkjet printer itself.

The initial ADA was carried out on MAPI AVA in GBL at 1mol. concentration, this was the highest concentration that produced stable results with the rheometer as there were issues with precipitation at the 1.2mol solution, so this was the concentration chosen for progression

to use on the inkjet with the hope that it would offer the best efficiency outcomes whilst still maintaining stability of the solution.
The optimised parameters for the GBL solvent on its own were used as a starting point for the tests carried out with the perovskite ink.

The droplet condition was important when examining the quality of the deposition as it had a significant effect on multiple factors including the uniformity of the layer deposited and the volume of solution or 'ink' deposited. Both these factors had a significant impact on the quality, and efficiency, of the cells produced during subsequent testing. For example, any nozzle clogging that led to the droplet volume being reduced meant that an insufficient volume of perovskite was deposited resulting in reduced functionality of the cells.

Therefore, the ADA feature that enabled optimisation of the piezoelectric wave as well as print parameters on the PixDro software, was used to determine the optimal parameters for the inkjet printer to be working at to produce a clean and stable droplet condition, producing the best print layer possible. This was done by running a series of tests altering various parameters on the advanced drop analysis software on the inkjet printer.

Whilst gaining familiarity with both the printer itself and the ADA software as well as the behaviour of an ink in the inkjet system, the first tests were carried out using commercial black HP printing ink to minimise health and safety risk factors. As well as being non-hazardous this ink had an added benefit of being highly pigmented. This aided the learning process further by making it very clear whether the flow rate of the ink had been calibrated correctly, by changing the level of back pressure within the ink reservoir on the printer, as well as which areas of the inkjet needed cleaning to maintain good jetting of the nozzles due to the high visibility of any residual ink on the printhead after cleaning was carried out.

Features such as the backpressure of the ink chamber as well as the parameters of the piezoelectric wave and their effect on the behaviour of the ink were explored at this point.

The backpressure of the ink chamber affected the flow rate of the ink, therefore regulating the volume that was deposited. If the back pressure in the chamber was too low, the ink would 'pour' rather than jetting in consistent and stable droplets. This would flood any cell being deposited onto as well as wasting a significant volume of solution. Therefore, the

backpressure of the chamber had to be maintained at a high enough pressure to prevent this uncontrolled flow.

Conversely, if the backpressure was set too high, it would cause bubbling in the ink chamber indicating that air had been drawn into the system as well as stopping any deposition of the ink from taking place. If this occurred, the backpressure would be immediately lowered to a suitable level and the system flushed though to purge the air.

Another aspect that affected the level of the back pressure needed was the number of nozzles in the printhead that were blocked. If a greater number of the nozzles were blocked and in need of cleaning a higher backpressure would need to be maintained to prevent flooding. This would help to indicate a need to clean the printhead.

Therefore, the backpressure was a factor that was constantly monitored throughout working with the printer to ensure that it was always held at the optimum level.

When considering the piezoelectric wave itself there were many different aspects to be taken into consideration. Each of these factors had varying levels of influence on the droplet produced and all were explored at this stage of the testing process.

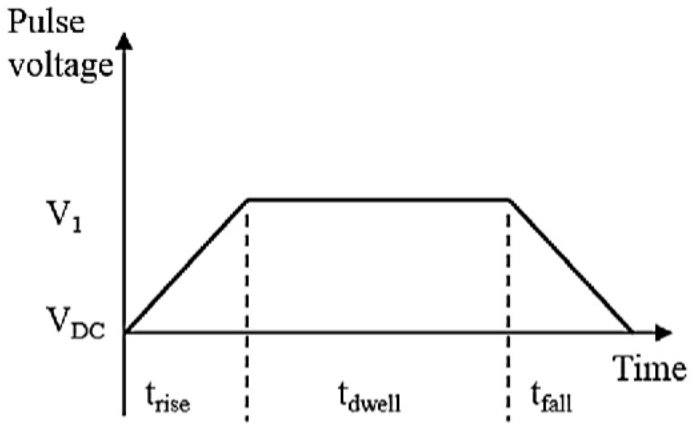

Figure 16 – image of individual wave pulse of piezoelectric printhead [28]

Figure 16 shows the pattern of an individual wave pulse of the piezoelectric printhead. The adjustable parameters of the piezoelectric wave are illustrated on the above figure,14. The peak time of the wave is shown as the dwell time, the horizontal middle part of the wave line. The rising and falling edges of the wave are shown by the sloped lines at either end of the wave pattern and notated by t_{rise} and t_{fall} respectively. The voltage of the wave is shown on the y-axis of the graph. These features of the piezoelectric wave were all parameters that could be adjusted on the inkjet printer as part of the advanced drop analysis and were the focus of the optimisation of the printing parameters for the 'inks'.

Parameters of the wave optimised through testing:

- Peak time of the wave
- Rising edge of the wave
- Falling edge of the wave
- Voltage of the wave

For the various aspects of the wave including the rising edge, falling edge and peak time a series of tests were run to create an optimised wave pattern producing a stable and round droplet with consistent volume. The previously mentioned parameters were altered by changing the time that that aspect of the wave took.
For each test, changing one parameter at a time and keeping the rest as the optimised values from the previous stage of testing, a drop analysis was run where the parameter in question was reduced to a minimum point specified and then ramped up from this point through a range of values to a specified maximum to ascertain the optimum amount of time taken for the parameter within the selected range.
This was achieved by using the 'Recipe' tab of the PixDro software. It was this tab that gave full malleability of the parameters and allowed for the ADA to be carried out.

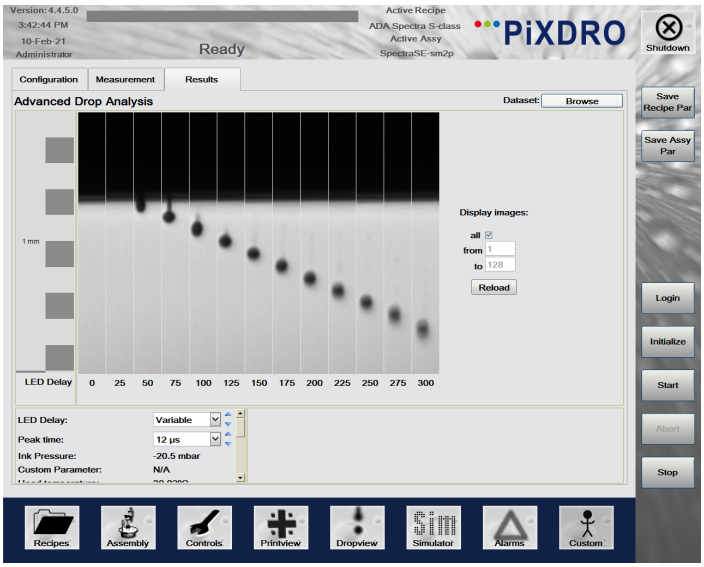

Figure 17 – Advanced drop analysis results window example

The image in Figure 17 illustrates the view of the ADA results offered by the 'recipe' tab on the PixDro program that was used to carry out the advanced drop analysis.

After working with the commercial HP ink to gain familiarity with the software and how to alter the parameters, the first tests were run with the GBL solvent on its own. This solvent was easy to optimise the parameters for, as there was a clear set of parameters that produced a much better droplet than any other. These parameters were:

	Rising edge (µs)	Peak time (µs)	Falling edge (µs)
GBL	8	16	3

Table 2 *Optimum parameters for GBL droplet formation*

These values were then used to inform the ranges selected for the testing of the GBL MAPI and GVL MAPI perovskite inks.

4.3.1 Peak time optimisation

The first parameter to be examined was the peak time of the wave. It was shown during initial familiarisation work with the commercial ink to have a substantial effect on the quality of the droplet formed, so was selected as the primary parameter when working with the GBL MAPI.

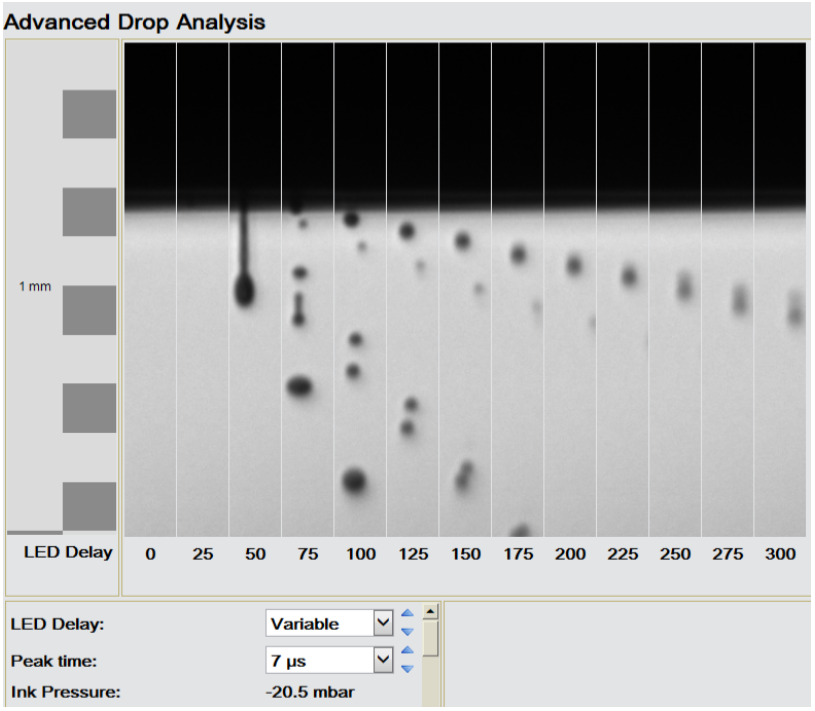

Figure 18 – Image of one droplet over time at a set peak time of 7µs

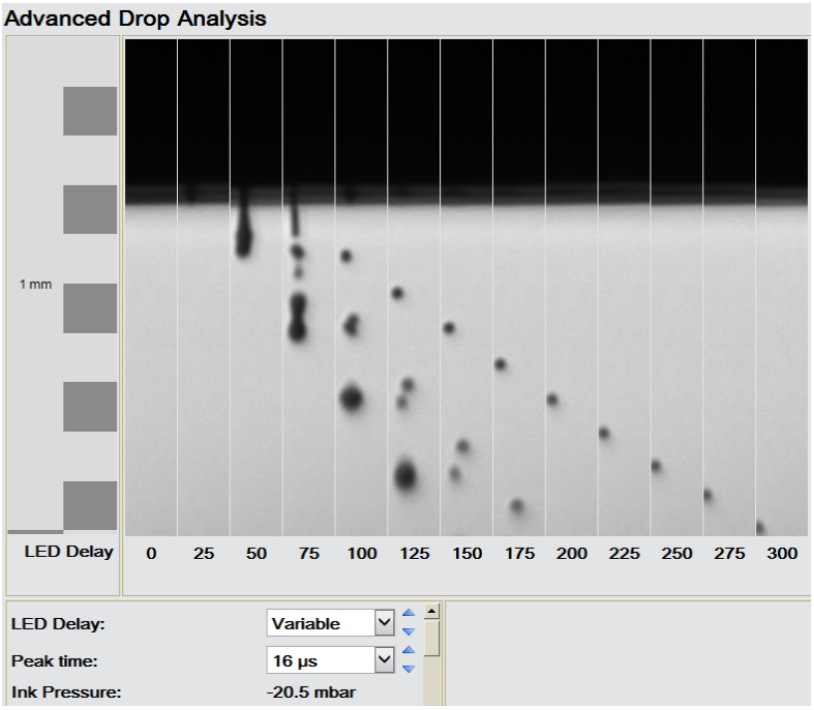

Figure 19 – Image of one droplet over time at a set peak time of 16µs

Figures 18 and 19 show different selected peak times of 7µs and 16µs respectively, set against a variable LED delay time. This variable LED delay indicates that a series of photos of one single droplet were captured as it fell past the camera. Therefore, the figures illustrate

the path of a single droplet moving past the camera, the droplet flight, at a selected peak time of the wave.
However, both of the above figures also feature ‘satellite’ droplets – smaller droplets also falling with the main droplet and resulting from a non-optimal, longer liquid thread at the point of the ink leaving the nozzle. [29]

As shown by the figure 19, the peak time was tested over a complete range from 5µs to 20µs. This difference in the time of the peak of the wave was found to have a significant effect on the quality of the droplet produced by the Spectra print head when working with the GBL MAPI.

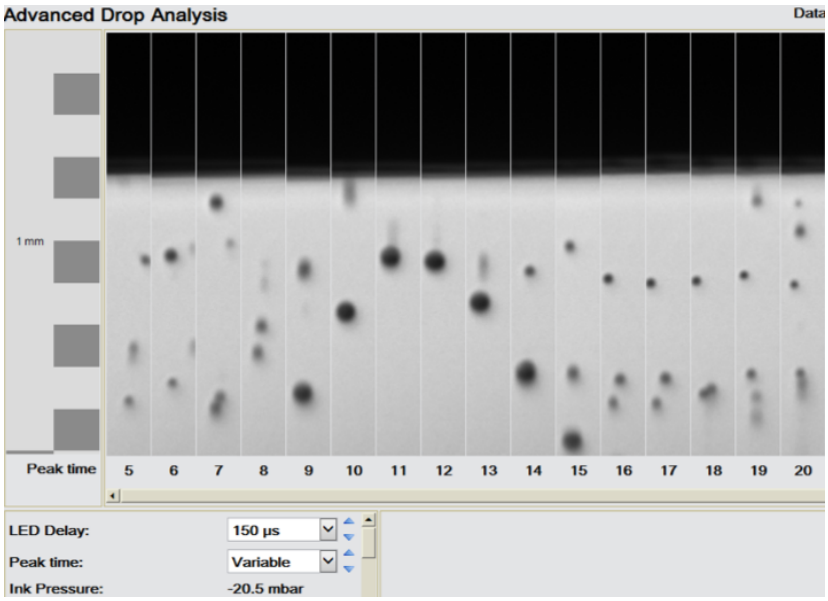

Figure 20 – Image of multiple droplets at 150µs LED delay during peak time testing

Figure 20 above shows how the ADA software was run to achieve the optimisation of each of the parameters. The image shows a snapshot at an LED delay time of 150µs from the point of the droplet leaving the nozzle of several different droplets all jetted with a different peak time of the wave. Here all other parameters remained the same throughout this jetting cycle, but the peak time was varied. This provided a clear comparison between the different peak times and showed the significant effect this parameter had on the behaviour of the droplet. As shown, the more extreme ends of this range from 5µs to 20µs do not produce a main droplet at all; there are many small ‘satellite’ droplets present, but no primary droplet. As the range

moves closer to the optimum value a droplet does form and fall from the nozzle but still with small satellite droplets or instability. This instability is indicated by the oval shape of the droplet, for example at 14µs. The optimum value for the GBL based ink is 12µs as shown by this being the value that produced the cleanest and most stable droplet.

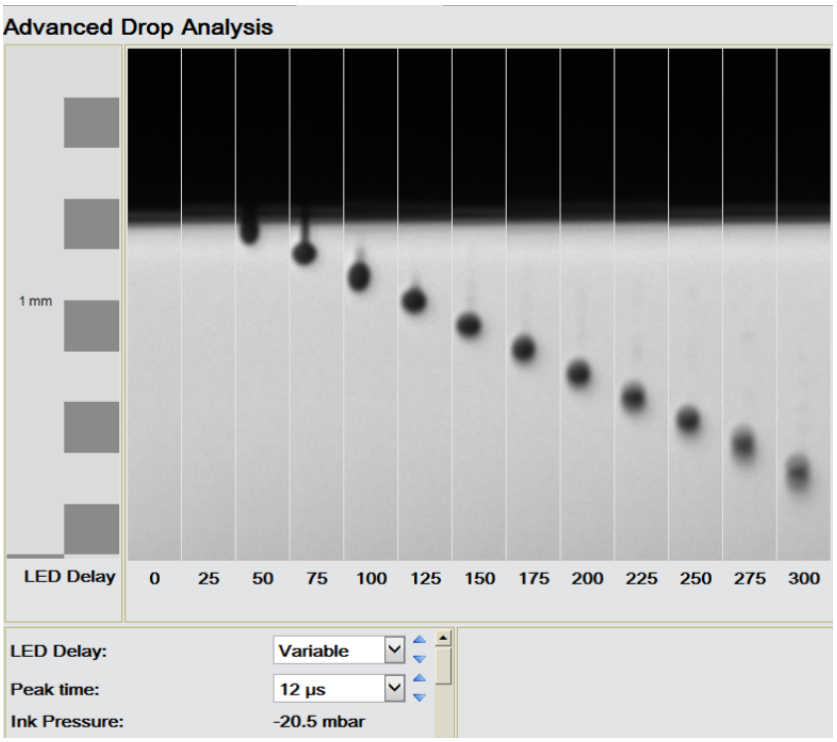

Figure 21 – image of one droplet over time at optimised peak time of 12µs

Figure 21 displays one droplet over time. The varied LED display time indicates that the figure shows several images of the same droplet as it travels past the camera. It illustrates the behaviour of the optimised droplet for this initial parameter testing.
Moving forward with the next set of parameters to be tested, the peak time remained at 12µs throughout.

4.3.2 Rising edge optimisation

The next parameter tested was the rising edge of the wave which also heavily influenced the behaviour of the droplet. This was varied in the same way as the peak time of the wave with testing starting at a specified minimum value and moving up through a range until a maximum value. All other parameters remained the same. The figures below illustrate the behaviour of the droplet when the rising edge of the wave was varied.

Figure 22 illustrates the range of values tested for the rising edge parameter of the wave. The range selected was between 1µs and 10µs. It shows 10 different droplets all captured at 125µs LED delay. Although the rising edge had a less significant effect on the speed of the droplet than the peak time of the wave (as shown by the main droplets all being at a more similar height at 125µs LED delay) there was significant change in the volume and stability of the droplet produced when varying the rising edge of the wave.

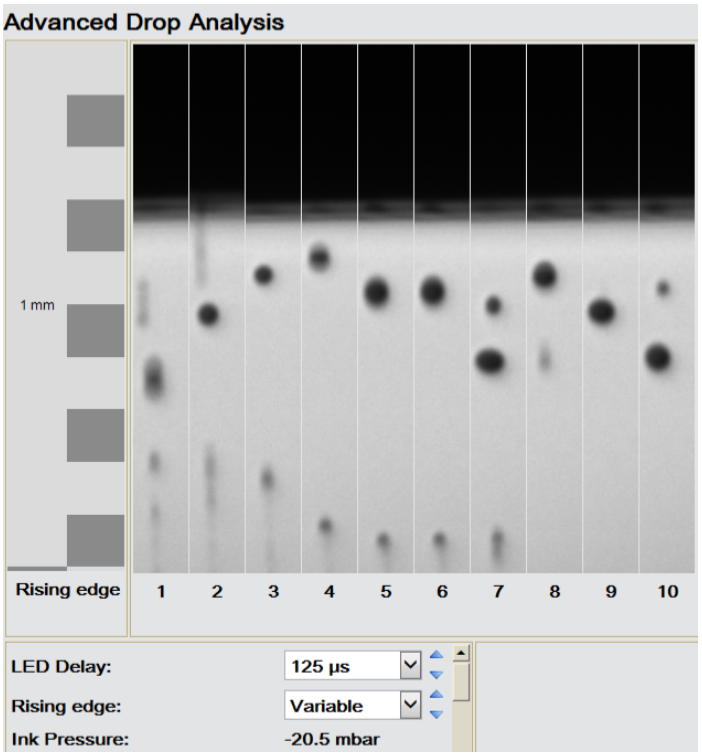

Figure 22 – Image of multiple droplets at LED delay of 125µs during rising edge testing

The optimum value for the rising edge was 9µs as shown by Figure 23 below.

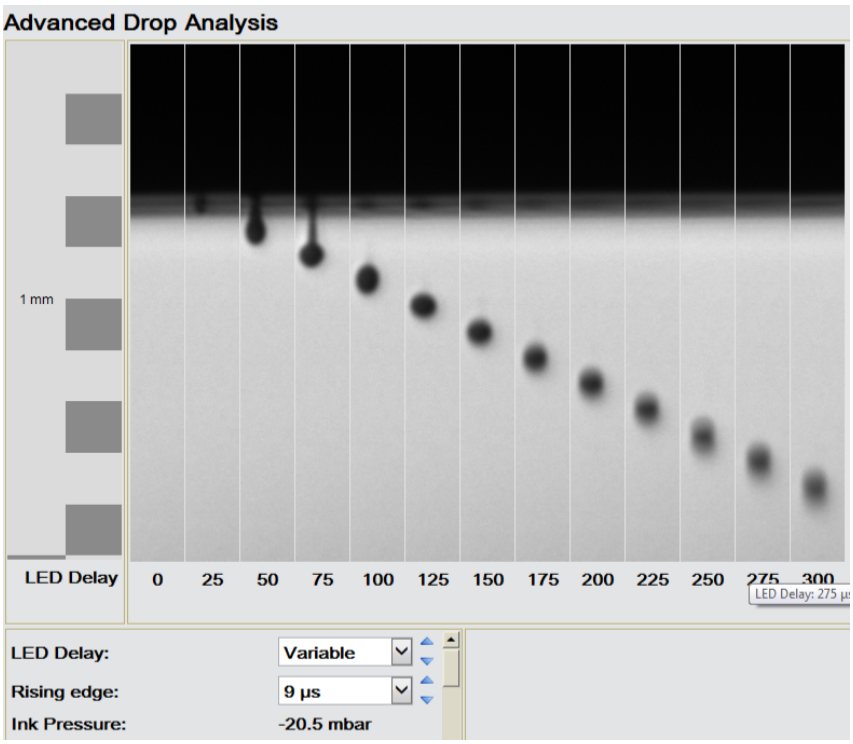

Figure 23 – Image of one droplet over time at the optimised rising edge value of 9µs

4.3.3 Falling edge optimisation

The next parameter examined was the falling edge of the wave. This was done in the same manner as the rising edge testing. The range selected was between 1µs and 10µs, based on the optimal values obtained during initial testing done with the GBL solvent in isolation. The optimum droplet was produced at 3µs when testing this parameter in isolation. Although there was still a low level of droplet instability with this parameter even in its optimised condition, as shown by the small satellite droplet still present, it still produced a round stable droplet when utilised in tandem with the other optimised parameters such as the voltage which was optimised following the rising, falling and peak times of the wave.

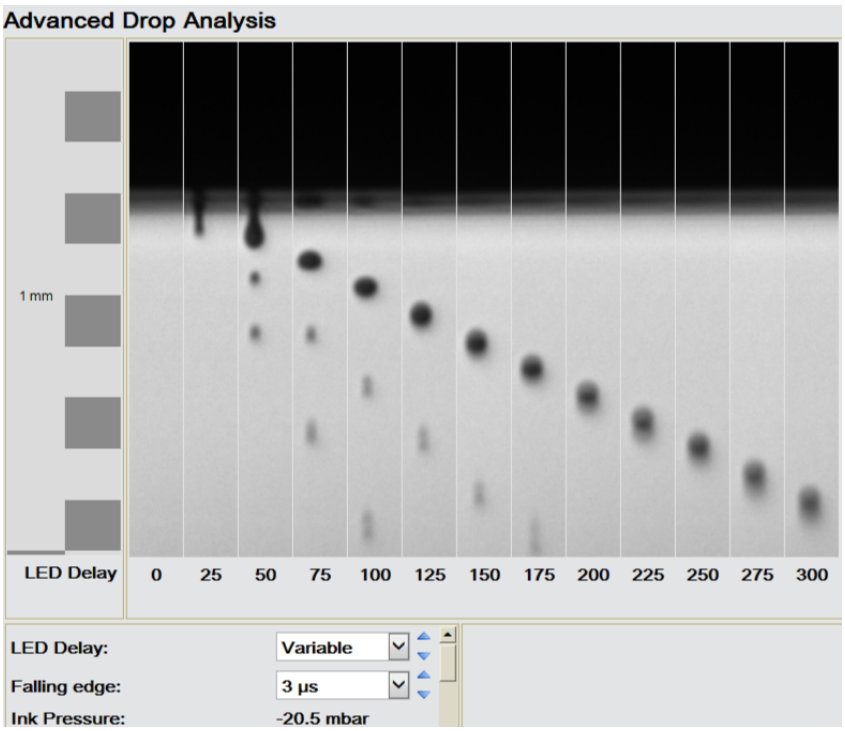

Figure 24 – Image of one droplet over time at a falling edge value of 3µs

Rising vs falling edge matrix – waveshape optimisation:

When displaying the data obtained through the advanced drop analysis there were two different types of images that could be used. The figures 25 and 26 are two images illustrating snapshots of the behaviour of ten different droplets as they fell past the camera at an LED delay time of 125µs.

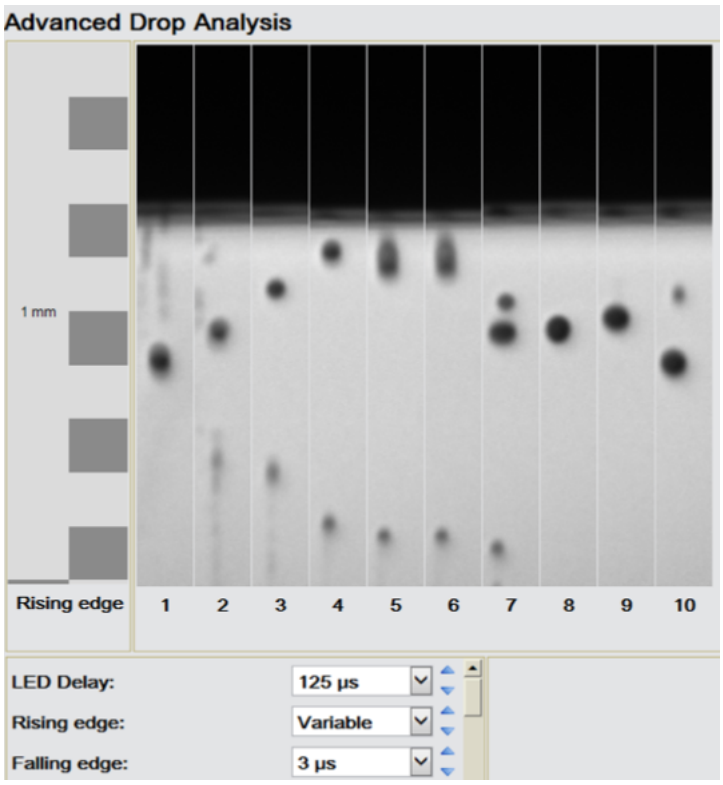

Figure 25 – Image of rising vs falling edge matrix with falling edge fixed at 3µs

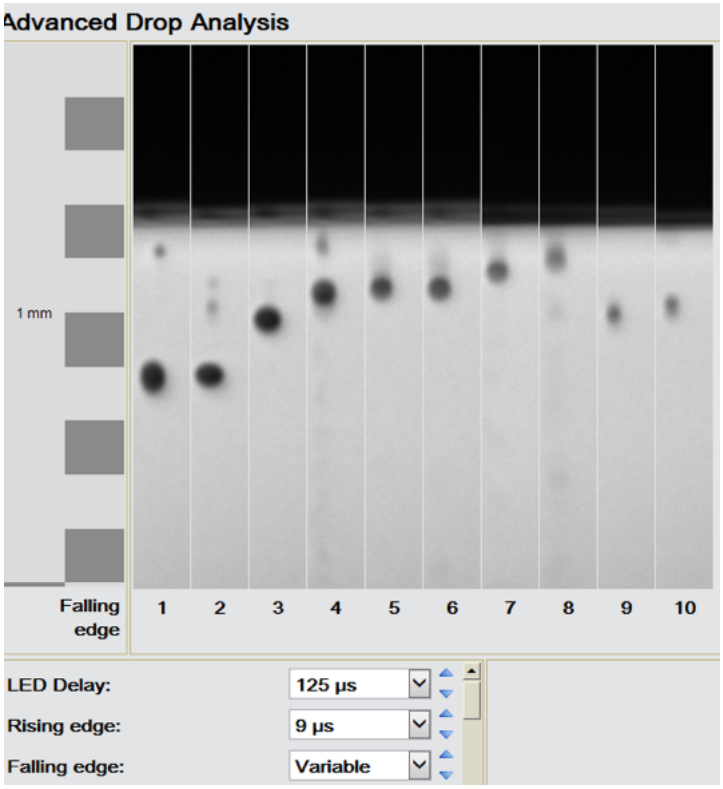

Figure 26 – Image of rising vs falling edge matrix with rising edge fixed at 9µs

The two images 25 and 26 above show how the rising edge and then the falling edge were tested in relation to each other using a matrix feature on the ADA software. The optimised peak time value was used. The variables for this test were both the rising edge and falling edge of the wave and the range was from 1µs to 10µs for both parameters. As shown by Figure 23, changing the rising edge of the wave had a significant impact on the droplet produced. When testing the rising and falling edge in relation to each other it was determined that the optimum droplet was produced when the rising edge was 9µs. The variation of the falling edge of the wave produced a less dramatic effect on the droplet formed, however there was still a clear optimum value which was 3µs as this produced a clean, spherical droplet with no satellites.

In optimising the rising edge, falling edge and the peak time, the shape of the wave was determined.

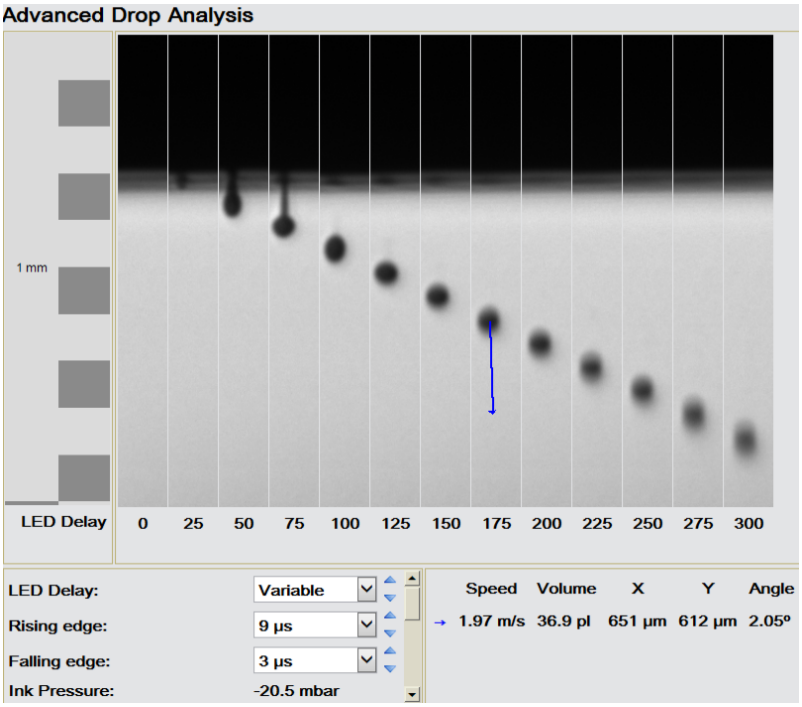

Figure 27 – Image of optimised rising and falling edge wave parameters for GBL MAPI

Figure 27 shows the ADA run with the rising edge, falling edge and the peak time all optimised. It shows one droplet of consistent volume falling almost directly downwards from the nozzle with no satellites or distortions in its shape. Each snapshot shows the same droplet travelling past the camera over a period of time as shown by the LED delay.

This image also showcases another feature of the ADA software that enabled additional analysis of the droplet. This was the ability to record the speed and volume of the droplet as well as its angle of deviation from the vertical.
This gave added insight into the behaviour of the droplet and allowed further comparison between the GBL and GVL based solutions.
In Figure 27 the volume of the optimised droplet of the GBL MAPI solution is 36.9pl and the image shows that the volume remains constant throughout its fall from the print head to the print deck.

There were still some issues with the stability of the droplet as shown in the above figure by the fact that although the droplet is round and has no satellites, it does not fall straight from the nozzle, and it becomes blurred in the image as it moves past the camera as shown in the images of the LED delay from 200 – 300µs. This blurring effect perhaps indicates movement on an angle of the droplet or the increasing velocity putting it out of focus.

	Rising edge (µs)	Peak time (µs)	Falling edge (µs)
MAPI AVA GBL	9	12	3

Table 3 *Optimum parameters for MAPI AVA GBL droplet formation*

4.3.4 Voltage optimisation

The voltage was tested over a very large range of values ranging from 10 volts all the way up to 125 volts. The software split this into two sections – low voltage, ranging from 10 to 70 volts and then high voltage from 70 volts upwards.
The voltage used also had a significant effect on the droplet as shown by the following images. At very low voltage – such as 15 volts the droplet production was very unstable. Figure 28 At 50 volts, a middle value, there was no droplet present at all. Figure 29

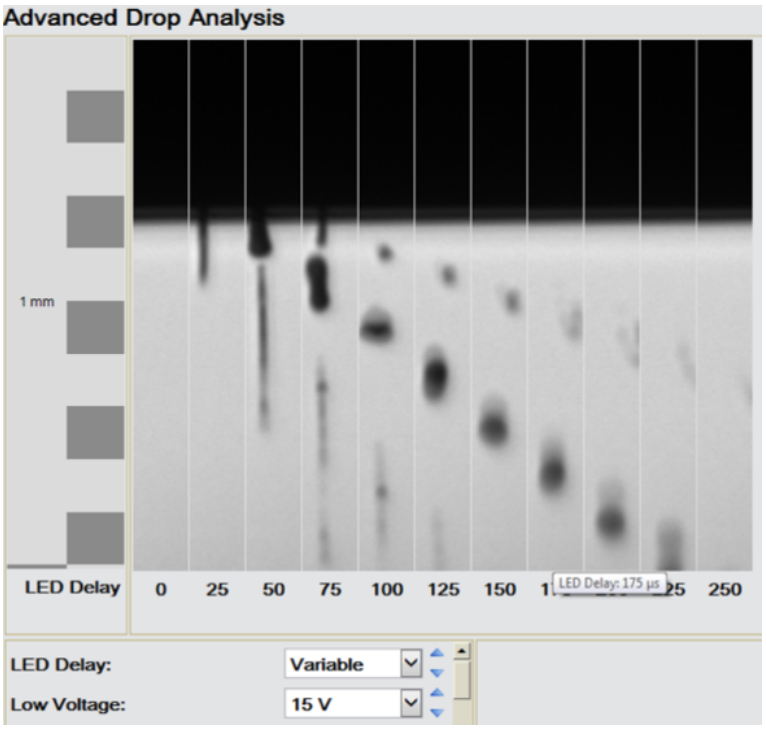

Figure 28 – Image of one droplet over time at non-optimised 15V

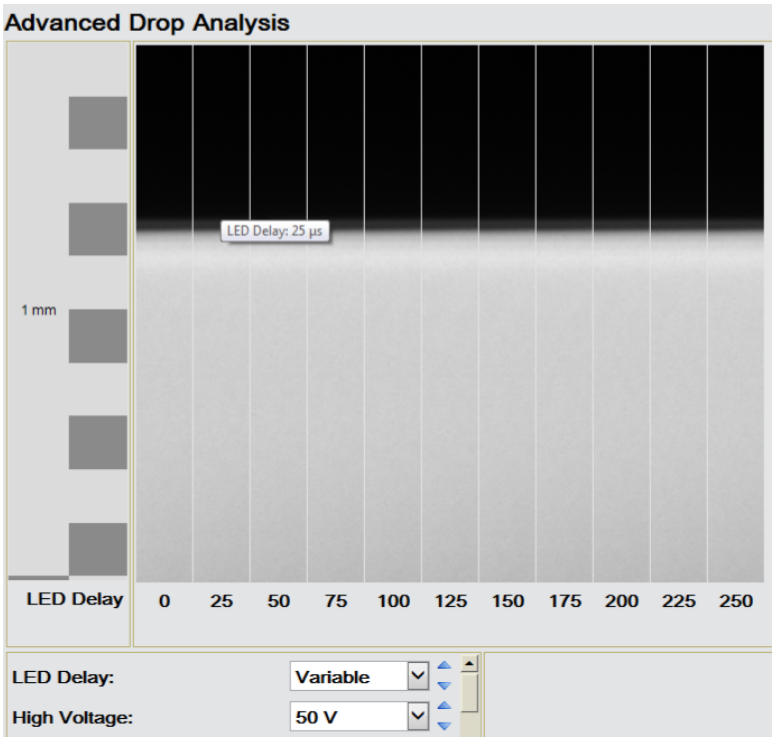

Figure 29 – Image showing no droplet jetting at non-optimised 50V

Below in Figure 30 is an image of the optimised value for the voltage of the wave when working with the GBL MAPI solution. The value shown here as the optimised value for the

voltage is 65volts however this fluctuated between 65 and 70volts in practice and the droplet was optimised each session when working on printing.

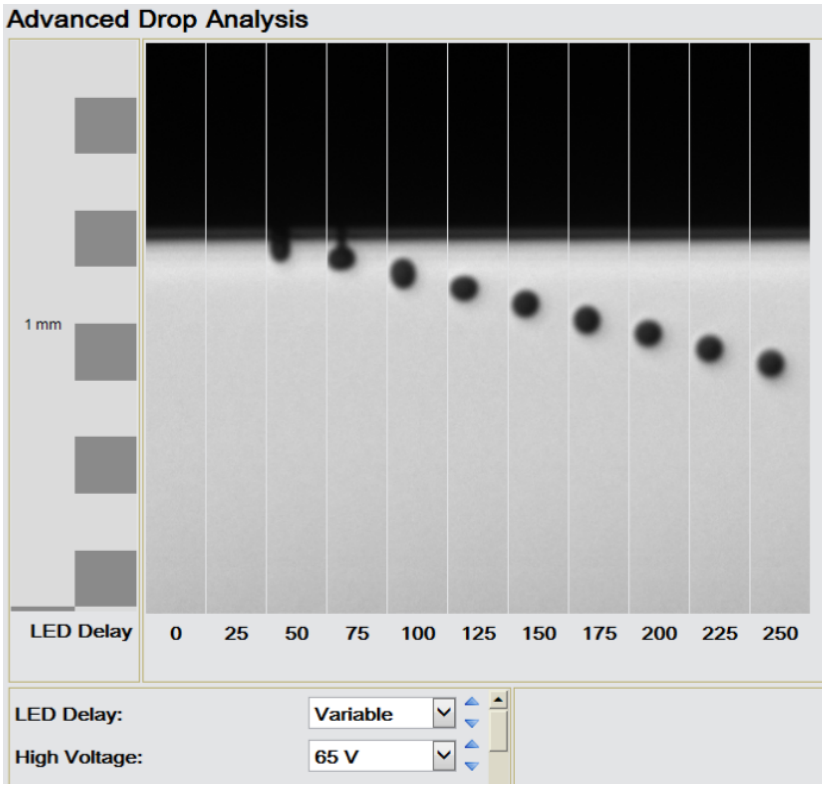

Figure 30 – Image showing one droplet over time at optimised voltage value of 65V

Whilst the voltage was the final aspect of the wave to be optimised, additional work was done with the GBL based perovskite solution. The temperature of the Spectra print head could be altered so tests were run to examine the effect of this on the behaviour of the ink as well as the droplet production. Tests were run with the print head at room temperature (20°C) as well as 30°C and 60°C. However, it was found that increasing the temperature of the printhead beyond 30°C was detrimental to the jetting of the ink from the nozzles.

However, the main issue with the GBL was the stability of the droplet once these optimal parameters were realised, meaning that if the printer was left jetting for a sustained period of time, for example 20 minutes, with the optimised parameters the quality of the droplet often deteriorated or stopped jetting at all.
The parameters would then need recalibrating to return the droplets produced by the printhead to the ideal state. Therefore, it was difficult to define a set of parameters that was consistently correct for the GBL solvent system.

This lack of stability of the GBL MAPI solution posed a problem when ascertaining the viability of using this solvent as the base for the ink when printing. To print the perovskite onto the solar cell the inkjet printer would need to be jetting for a sustained period of time, and throughout this deposit a uniform volume of perovskite across the entire active area of the cell.

4.4 Advanced drop analysis (ADA) – GVL MAPI optimisation

The tests carried out on the GVL MAPI solution were conducted in the same manner, as the GBL based solution, working with assumed values initially and optimising the peak time of the wave first. The assumed values were taken from tests run with the GVL solvent individually and these combined with the results from the optimisation of the GBL MAPI solution informed the ranges that were tested for the GVL MAPI solution.

4.4.1 Peak time optimisation

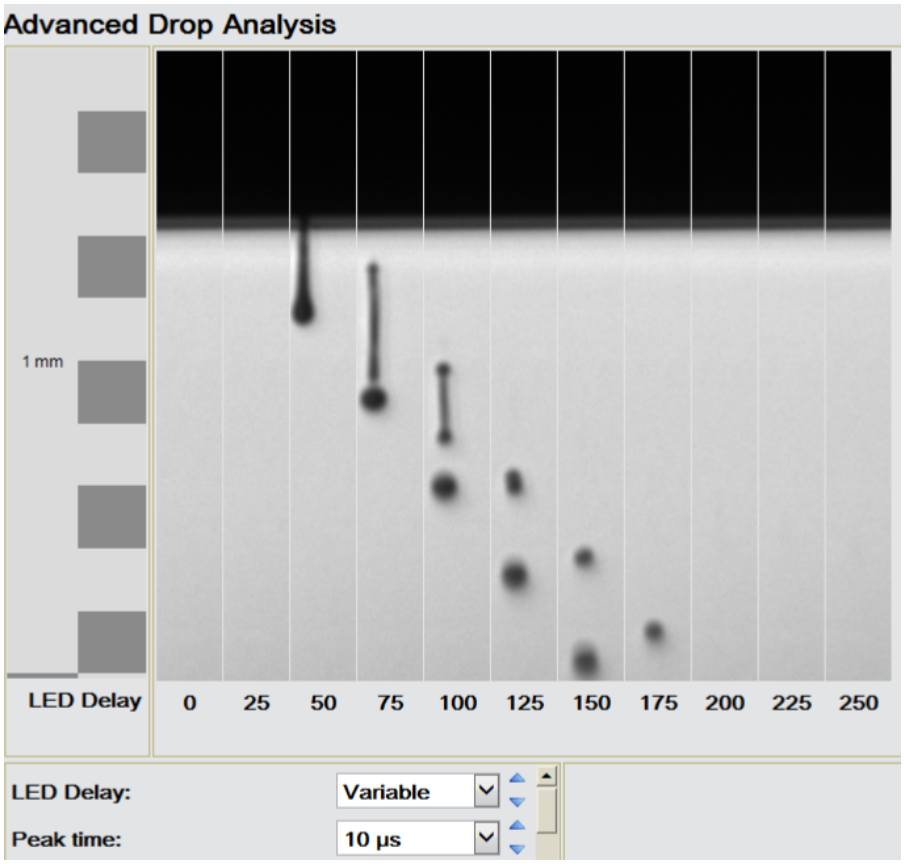

Figure 31 – Image of one droplet over time at a peak time of 10µs

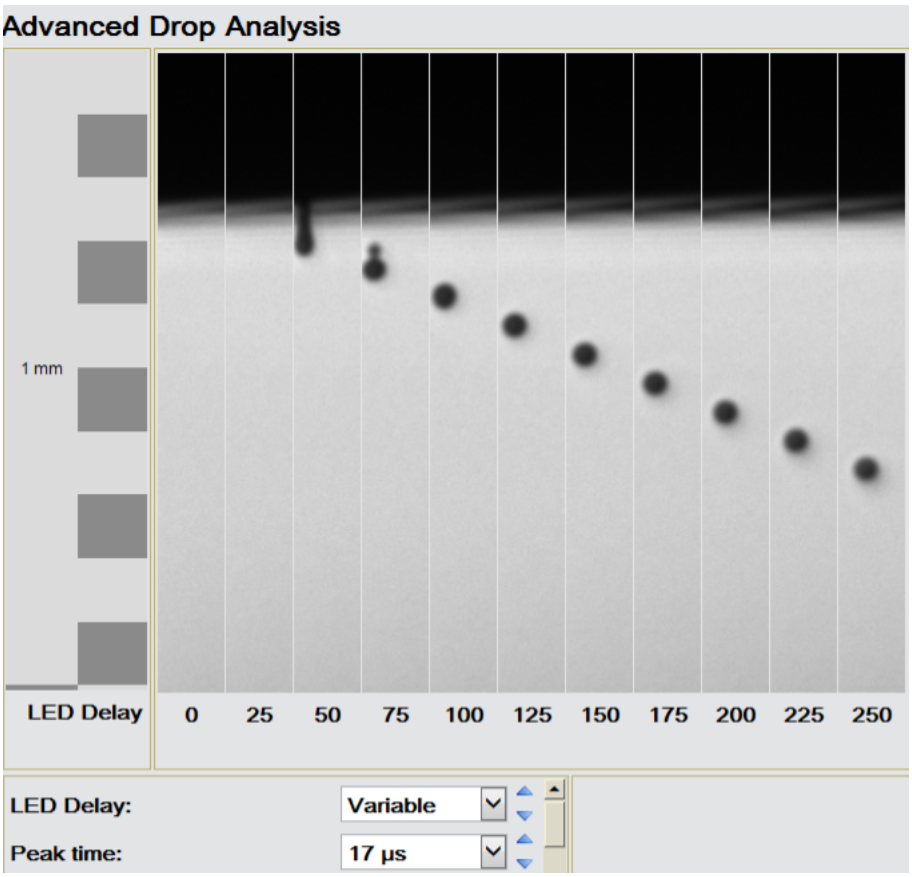

Figure 32 – Image of one droplet over time at optimised peak time of 17µs

Figure 31 shows the droplet at 10µs peak time showcases the splitting of the droplet into two smaller drops, occurring when the wave parameter is not optimised. This leads to an inconsistent volume of ink being deposited onto the cell whenever this nozzle is working and can also lead to a messy print. Figure 32 shows the optimised peak time for the GVL MAPI solution of 17µs. This could be due to the increased viscosity of this solution when compared to the GBL based solution. A longer peak time meant that the maximum voltage value of the wave was applied for longer.

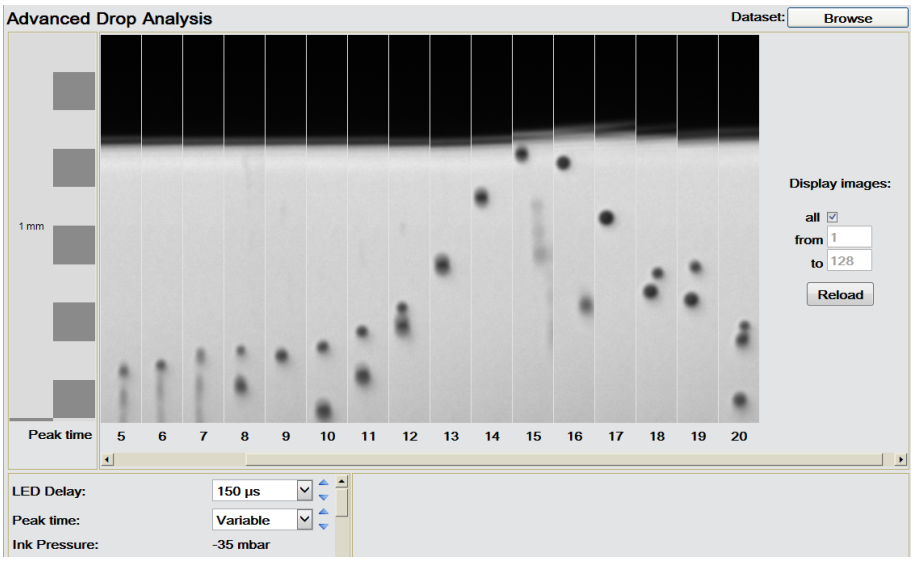

Figure 33 – Image of multiple droplets at LED delay of 150µs during peak time testing

The figures 31, 32 and 33 show the clear difference in the droplet quality as the peak time of the wave was optimised. Tests were conducted within a range from 5µs to 20µs. At 12µs, the optimised peak time for the GBL solution, the droplet produced was not ideal. There were consistently satellite droplets, as shown in Figure 33. The optimised peak time for the GVL MAPI solution was much higher at 17µs, as shown in Figure 32.

4.4.2 Rising edge and falling edge optimisation

As with the GBL MAPI the next aspects of the wave to be optimised were the rising and then falling edges. The rising edge for the GVL MAPI solution was very different to the rising edge of the GBL based solution. As shown by the image below, Figure 34, the optimised value for the rising edge was 2µs. The falling edge value remained the same as for the GBL solution, therefore, raising the potential that this parameter did not have a significant effect on the droplet formation.

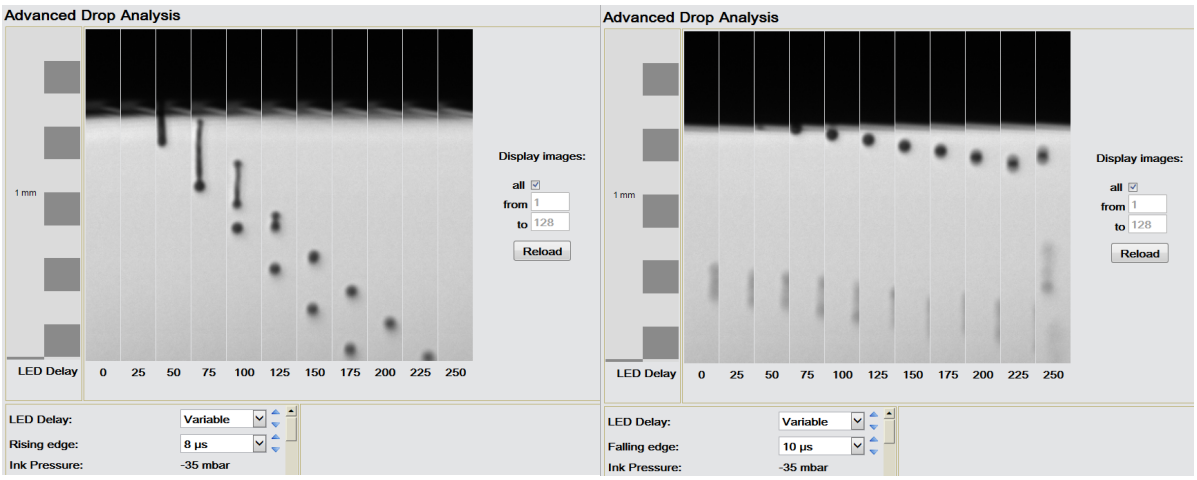

Figure 34 – Images of non-optimised rising and falling edges of the wave (one droplet over time)

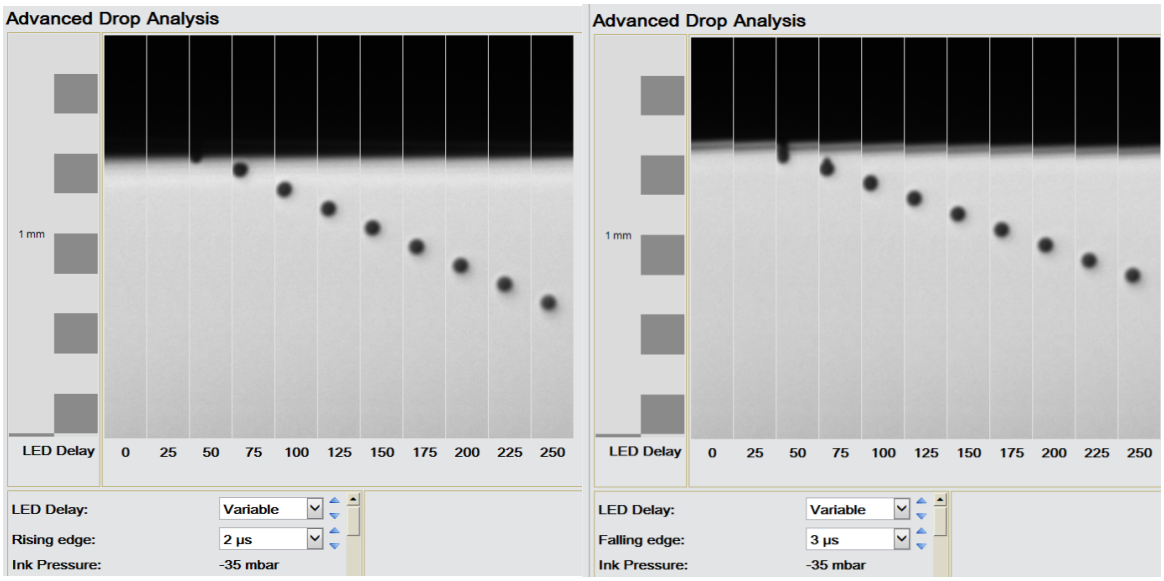

Figure 35– Images of optimised rising and falling edges of the wave (one droplet over time)

Figures 34 and 35 show that for the rising edge the optimum parameter was 2µs and for the falling edge the optimum was 3µs.

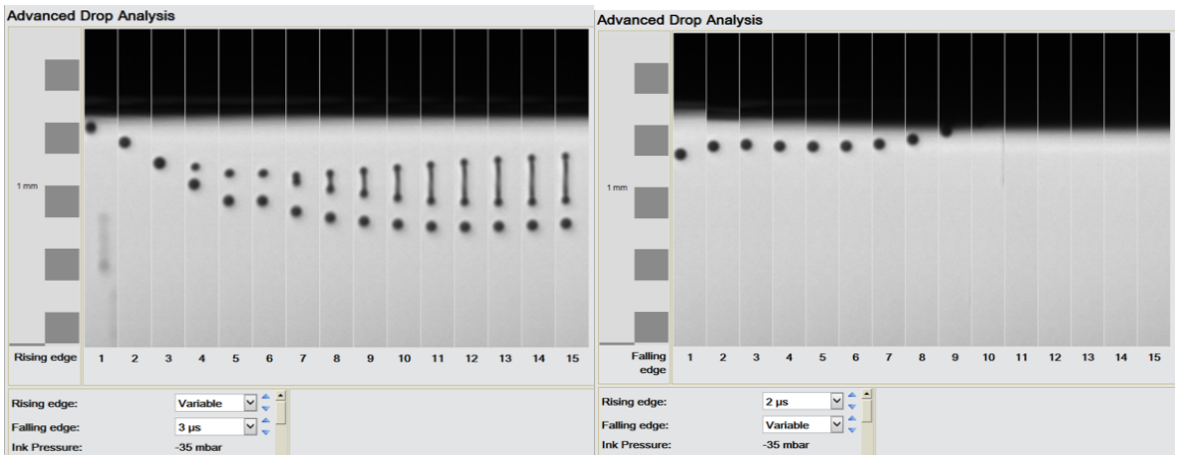

Figure 36 – Images of rising and falling edge matrix results

Figure 36 above taken using the matrix feature of the ADA software, and Figure 35, serve to illustrate that the rising edge has a greater effect on the droplet formation than the falling edge. This is shown by the variation of the droplet formation when the falling edge is fixed at its optimum value, but the rising edge is varied. Satellite droplets formed at higher rising edge values as well as elongated droplets that would have a negative impact on the print quality due to a lack of uniformity. However, when the rising edge value was fixed at its optimum and the falling edge value was varied there was very little change in the formation of the droplet until 10µs when a droplet no longer formed.

	Rising edge (µs)	Peak time (µs)	Falling edge (µs)
MAPI AVA GVL	2	17	3

Table 4 *Optimum rising edge, peak time and falling edge parameters for MAPI AVA GBL droplet formation*

4.4.3 Voltage optimisation

For the GVL perovskite solution specifically there were two different voltages that produced a good droplet. During the low voltage testing of the GVL MAPI it was found that at 70 volts there was also a good stable droplet produced. However, it was not as spherical as the droplet at 120 volts which was the final value recorded as the ideal parameter for this ink.

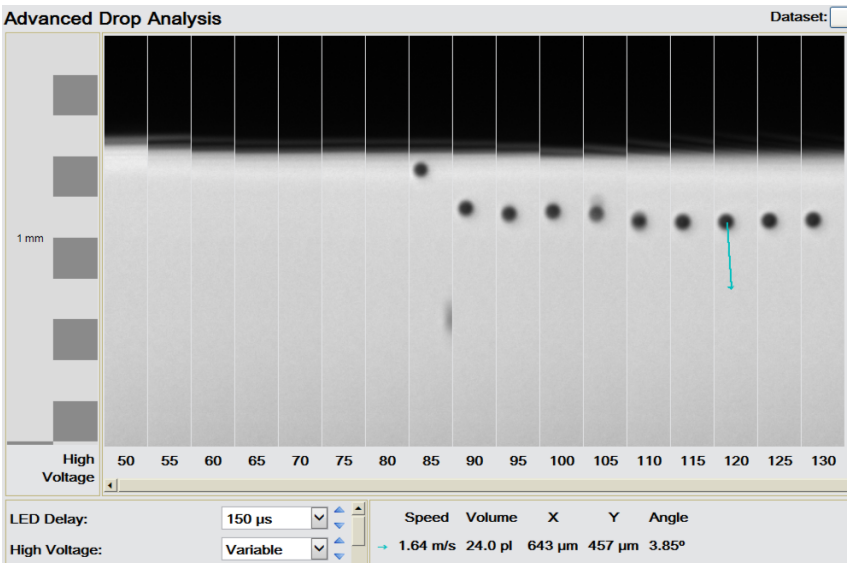

Figure 37 – Image of multiple droplets during voltage optimisation

4.5 Volume of the droplet exploration

As well as showcasing the ideal droplet voltage the above image, Figure 37, also shows the volume of an optimised droplet. The optimised droplet volume for the GVL MAPI was 24pl.

This is supported by the graphs below that show a comparison between the recorded droplet volumes at 10µs and 17µs peak times. The line graph at 10µs shows that although the droplet produced has a much higher maximum volume it is clearly unstable as shown by the reduction in volume as it falls. In contrast the droplet at 17µs remained steady at approximately 24pl for the duration of time that it was visible to the ADA camera. (Figure 37) This much higher value for the total volume also occurs due to satellite droplets occurring. Meaning it is the total value of all ink droplets visible to the ADA camera not just for one droplet as with the value for 17µs.

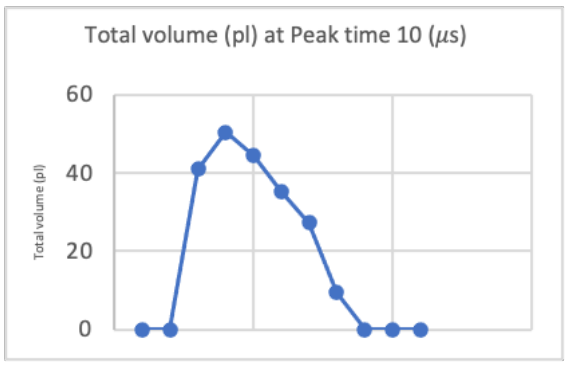

Figure 38 – Graph of the variation of volume of droplet over time at a peak time of 10μs

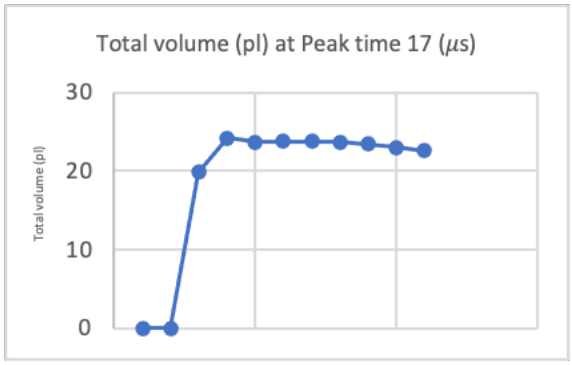

Figure 39 – Graph of the variation of volume of droplet over time at a peak time of 17μs

This data in Figures 38 and 39 also serves to highlight that the volume of the optimised droplet was different for the two solvent systems. For the GBL MAPI the volume was approximately 37pl, significantly higher than for the GVL MAPI solution which was approximately 24pl.

One reason for this could be the need to work at a higher back pressure when working with the GVL MAPI solution.
This seems counterintuitive given that the GVL MAPI solution has a higher viscosity so should need less back pressure to stop the flooding effect.
However, increased nozzle clogging, either due to a continual build-up through sustained usage of the Spectra inkjet head as the tests were run, or the higher viscosity of the GVL based solution led to the need for a higher back pressure.

4.6 Comparison of the optimised parameters of GBL MAPI and GVL MAPI

The optimal wave parameters for the solutions were found to be different.
As the GBL perovskite solution was optimised first these parameters were the starting point for the optimisation of the GVL solution, meaning that these values informed the ranges used when testing the GVL MAPI solution. The table below lists the optimum wave parameters for the perovskite precursors using the GBL or the GVL solvent respectively.

	Rising edge (μs)	Peak time (μs)	Falling edge (μs)	Voltage (V)
MAPI AVA GBL	9	12	3	70
MAPI AVA GVL	2	17	3	120

Table 5 – Comparison of the optimised wave parameters for GBL and GVL based inks

One aspect of the optimisation process that was interesting to observe was that the peak time and rising edge had a much more dramatic impact on the quality and stability of the droplet produced than the falling edge or voltage of the wave across both solvent systems. The differences in the images shown above support this by illustrating the much more pronounced changes in droplet formation that occurred when changing the rising edge or peak time of the wave. This occurred even though the optimised values for these two aspects of the wave were very different.

Although the times for the rising edge and peak time of the wave were substantially different between the two solvent systems the total time of the wave was very similar.

This is shown by the fact that the greatest differences are between the values for the rising edge and the peak time as well as the similarities between the falling edge values. There is also a gap between the values for voltage however some lower voltages in the region of 70V were also stable for a short time for the GVL MAPI, the 120V was just observed as the optimum.

The same trend was followed in the droplet behaviour when comparing the different parameters but the actual parameters themselves were optimised at different values.

In that the same parameters had a greater or lesser effect on droplet performance but the optimised values of the parameters that had the greatest effect on droplet performance were very different.
This is intriguing and speaks to the difference that the GVL makes to the solution as the other materials were identical and the solutions were of the same concentration.

During the ADA analysis the greatest focus was on the wave and print head parameters. Although the temperature of the print head was altered, and its effect explored during this testing as well. However, the print deck temperature remained constant at room temperature throughout all the ADA testing done on the inks as the focus was on the behaviour of the droplet rather than the deposition itself.

4.7 Deposition of perovskite 'inks' using inkjet method

Having completed the optimisation of the jetting parameters of both the GBL and GVL based perovskite inks, the first attempts at printing with GBL and GVL inks were carried out. Initial printing attempts were deposited onto a plastic substrate covering the whole of the print deck of the inkjet printer. This was to minimise waste of the materials used to manufacture the carbon stack and also to maximise the number of tests that could be run on one substrate whilst gaining familiarity with the deposition process.

When printing onto the plastic substrate with the parameters optimised by the ADA, the print was very accurate and produced a distinct and uniform square each time. This proved that the inkjet method could be used to create very highly specific patterns/active areas using the GBL MAPI ink when not infiltrating a mesoporous layer. The square was 1cm^2 to simulate printing onto the carbon stack which, when working with individual cells, had the same active area.

Due to continued issues with the long-term stability of the GBL MAPI solution when it was jetting for multiple back-to-back tests on the plastic substrate, where it would often produce incomplete patterns, the decision was made to focus the printing optimisation on the GVL MAPI solution. This decision was made in light of the desire to explore the inkjet deposition method as a viable method of scale up for the carbon stack production process. The amount of intervention needed to maintain a stable droplet with the GBL MAPI solution meant that

depositing over a larger surface area, for example modules rather than cells, or carrying out a large number of cell depositions would not be feasible.

This had the added advantage of eliminating the need to work with GBL which due to the nature of the solvent was much more heavily controlled and harder to procure.
The GVL solvent was also a "greener" solvent than the GBL therefore making it additionally more desirable.

4.7.1 Printing onto glass

The first prints on glass were done onto the treated glass substrate with the TiO_2 layer also screen printed. The optimised parameters for the GVL MAPI ink were used and the print head was held at 20°C.
This approach was taken to gain experience aligning the printhead with the edge of the active area of the solar cell using the print head camera.
At this stage work was done to alter the amount of perovskite deposited. On the plastic substrate a much lower volume of perovskite was needed to produce a uniform layer fully covering the area needed. Due to the perovskite needing to infiltrate through the layers of the carbon stack a higher volume would be needed when producing the carbon stack solar cells.
To examine this, prints were carried out at varied resolutions.
The resolutions tested were:
300, 400, 500, 600, 700, 1000, 1100, 1200, 1500, 2000, 2250, 2500, 2750dpi
(Droplets per inch)

4.7.2 Printing onto the carbon stack

Due to the issues with stability encountered printing onto the plastic and glass substrates with the GBL based perovskite solution, only the GVL MAPI ink was used to deposit onto the carbon stack.
The stability of the GVL based ink meant that even with the time taken to complete set up and positioning of the cell and print head, the droplets would remain stable through the duration of a printing session.

When printing onto the carbon stack a much higher volume of perovskite ink was needed than when printing onto the plastic or glass substrates. This was to ensure that the perovskite

fully infiltrated the cell therefore enabling the device to work. Initial prints done onto the carbon stack had too little perovskite being deposited leading to poor performance on the solar simulator, with PCE values under 4%.

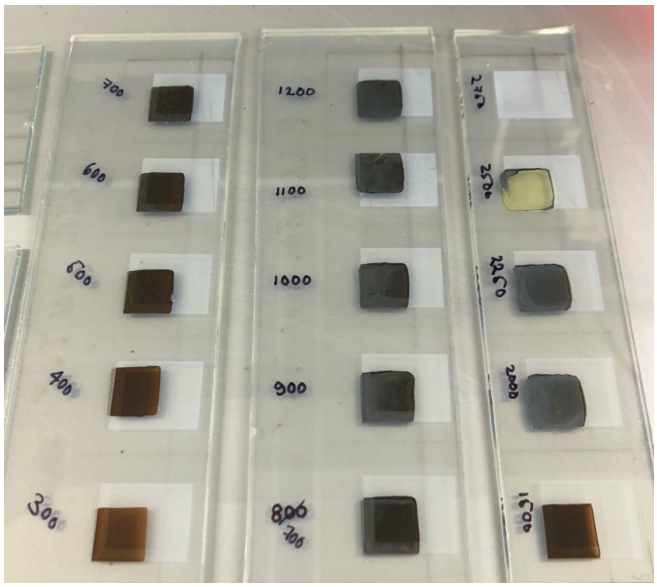

Figure 40 – Image of deposition onto glass substrate & TiO_2 layer at various resolutions

The first set of cells to be infiltrated using the GVL perovskite solution and tested on the solar simulator were infiltrated using a resolution ranging from 1500 to 2250dpi. This was as a result of the tests done on the glass substrate with the TiO_2 layer and the higher resolution values producing better films. (see figure 40) At these higher values films were black rather than brown indicating a better layer of the perovskite. For these initial tests on the carbon stack itself the active area of 1 cm^2 was still taken as the print area for the deposition. However, taking this approach produced cells that had significant overflow onto the surrounding substrate. This both wasted material and necessitated the extra post-printing step of scraping the excess perovskite from the glass substrate, prior to treating with the silver electrodes in preparation for the testing on the solar simulator.

With the first batch of testing, working cells were produced but with a low level of efficiency at this stage of the optimisation process.
The champion PCE value for this first batch of cells was 4.4% efficiency. All the cells worked, but others returned efficiencies as low as 1%. This was reflected in the fill factor of

the cells with the highest fill factor returning the highest efficiency values. For example, the cell with the lowest fill factor of 42% returned the lowest efficiency value of 1.1%.

The next batch of testing focussed further on the resolution of the print and therefore the volume of perovskite solution deposited onto the cells. Cells were produced that were infiltrated at resolutions of 2000, 2200 and 2400dpi. The print time for the active area of one cell of the highest resolution tested in this batch was recorded as 7 minutes and 38 seconds. This print time raised an issue with this production method as the time taken to print over a very small area was too high and when assessing this method and its potential for scale up this meant that on a larger scale the print time would be far too long to warrant employing this method of deposition.

Effort was subsequently made to reduce the print time and therefore increase the efficiency of this manufacturing method. One way this was addressed was by reducing the area of the print. The active area of the cells was 1 cm^2. As printing with this area had also previously caused problems with overspill, tests were run with reduced print areas to try to solve the problem of overspill whilst also reducing print time.

Prints were carried out with deposition areas of 0.9 cm^2 0.8 cm^2 0.7 cm^2 and 0.6 cm^2.
It was found that the print area could be reduced without compromising the efficiency of the cells however print areas as low as 0.6 cm^2 did have a detrimental effect on the functionality of the cells. This was due to the perovskite ink not infiltrating the cell fully therefore leading to cells of a very low efficiency or cells that were not functional. In the case of the 0.6 cm^2 print area the volume of perovskite deposited was too low due to the same resolution being used for all the prints carried out with this varying print area. Therefore, with a reduced print area the total volume of ink deposited was significantly reduced.

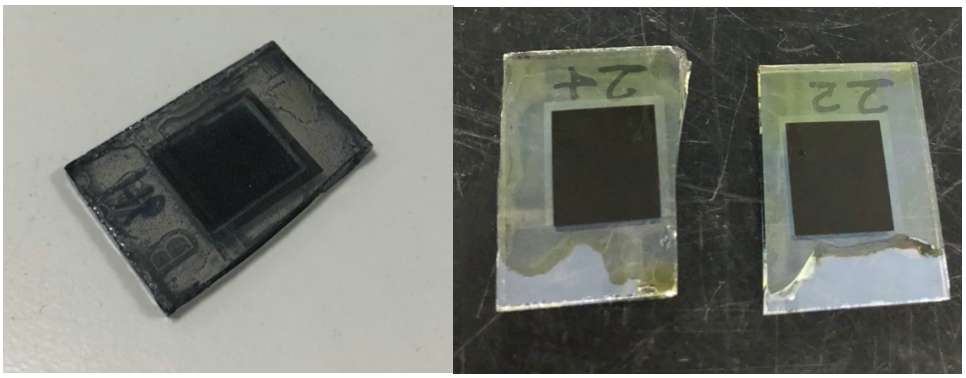

Figure 41 – Images of carbon stacks, post infiltration, showing overspill of perovskite

In terms of efficiency the optimal deposition area was found to be 0.9 cm² which reduced print time without compromising the infiltration of the cells.
This reduced print size also helped to minimise the overspill of the perovskite onto the surrounding substrate but did not eliminate the problem.

Tests were also run to ascertain the maximum speed at which the printhead could move without compromising the uniformity and overall quality of the print. For these tests the optimised values for the ADA were used along with the optimised deposition area of 0.9 cm².
The same resolution was used for a full batch of cells and the printhead speed was varied between 250 DPI (droplets per inch) and 500 DPI. The highest printhead speeds did detrimentally affect the efficiency of the cells produced resulting in efficiencies of as low as 5% with some cells also not working at all when measured under one sun in the solar simulator. However, the champion cells for this batch of testing managed to achieve 10.7% PCE at 300 Speed.
The highest speed of the printhead that could be used without detrimentally affecting the print quality was 350 so this was the speed that was used moving forward in testing.

Having ascertained the fastest print head speed that could be used, further testing focused again on the resolution of the print, this time printing in larger batches to also assess the reproducibility of the manufacturing technique.
A batch of six cells with the optimised parameters for the GVL solution and optimised print parameters of a 0.9 cm² deposition area and 350 print speed were then tested under the solar

simulator. This group of cells all also had the same resolution of the print, which was 2400 DPI, ensuring enough perovskite was deposited to fully infiltrate the carbon stack.

Cell ID	Direction	Efficiency (%)	Fill Factor (%)	Jsc (mA/Cm≤)	Voc (V) Stabilised
H1	Forward	10.27	63.97	20.95	0.77
H1	Reverse	10.83	64.01	21.13	0.8
H2	Forward	9.58	63.56	21	0.72
H2	Reverse	9.79	61.01	21.15	0.76
H3	Forward	7.63	48.97	20.81	0.75
H3	Reverse	7.4	48.92	21.01	0.72
H4	Forward	9.09	60.94	20.96	0.71
H4	Reverse	9.41	58.53	21.12	0.76
H5	Forward	9.26	59.56	21.01	0.74
H5	Reverse	9.75	58.51	21.18	0.79
H6	Forward	10.62	63.61	20.77	0.8
H6	Reverse	11.09	64.44	20.94	0.82

Table 6 – Results of batch H testing on the solar simulator

As shown above in Table 6 above, the champion cell of this batch produced a PCE of 11.09% and the worst performing cell produced a value of 7.4% for its efficiency. This also showed a greater level of consistency across the performance of a full batch of cells, compared to a wide range of values for PCE shown in earlier test batches. It was also the first batch with multiple cells with a PCE over 10%.

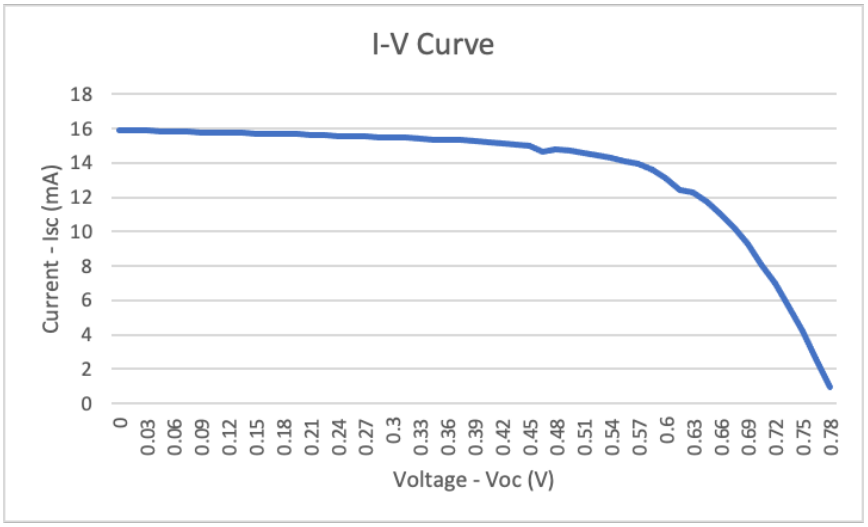

Figure 42 – I-V curve example using batch H data

The next batch repeated the exact same conditions but with a resolution of 2000, meaning a lower volume of perovskite solution was deposited. This batch produced slightly lower PCE values with the champion cell reaching 9% efficiency. The reproducibility of this batch was very good with the majority of the PCE values being within 2% of each other.

Cell ID	Direction	Efficiency (%)	Fill Factor (%)	Jsc (mA/Cm≤)	Voc (V) Stabilised
J1	Forward	8.38	57.62	19.87	0.73
J1	Reverse	5.77	39.5	19.62	0.74
J2	Forward	8.65	58.09	20.22	0.74
J2	Reverse	7.84	53.11	20.43	0.72
J3	Forward	9.02	59.93	19.91	0.76
J3	Reverse	6.96	46.14	19.79	0.76
J4	Forward	6.08	42.78	20.56	0.69
J4	Reverse	5.83	41.27	20.56	0.69
J5	Forward	8.54	58.55	19.43	0.75
J5	Reverse	6.07	42.36	19.17	0.75
J6	Forward	7.99	55.14	19.43	0.75
J6	Reverse	5.02	36.37	18.5	0.75

Table 7 – Results of batch J testing on the solar simulator

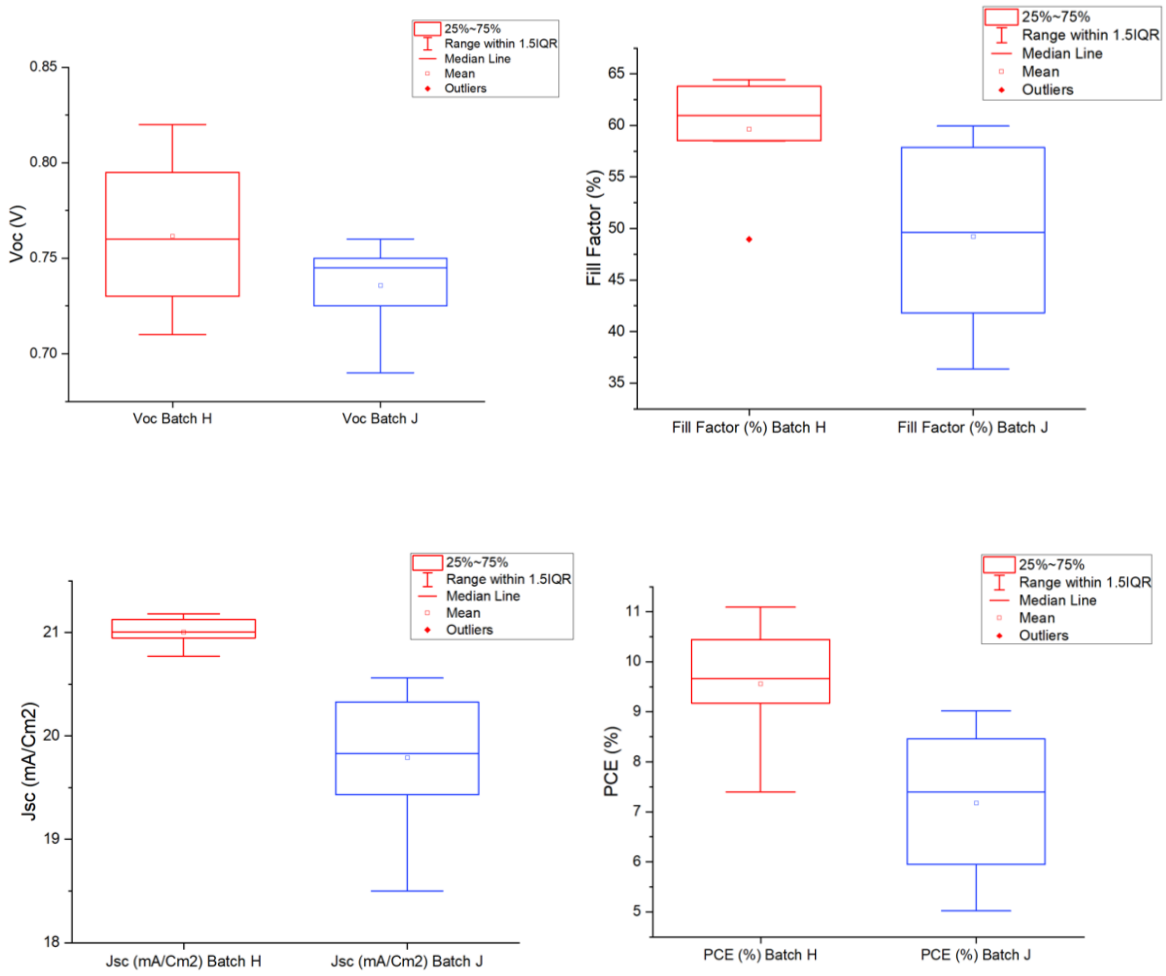

Figure 43 – Boxplots comparing the Voc, Fill Factor, Jsc and PCE of batches H and J

Another aspect that was assessed with later more highly optimised printing conditions was the stability of the cells manufactured using the inkjet technique. As such, the cells were repeatedly tested under the solar simulator; once on the day they were manufactured, then again on the fourth and eighth days since manufacture. The overall trend was that the efficiency values increased over the period of a week. Between tests the cells were stored in darkness which has been shown to have the same effect on carbon stack PSCs infiltrated using standard methods. [46]

Batch	PCE (%)	Fill Factor (%)	PCE Day 4	PCE Day 8
H1	10.27	63.97	11.08	11.71
H1	10.83	64.01	11.06	11.92
H2	9.58	63.56	9.92	10.16
H2	9.79	61.01	10.03	10.13
H3	7.63	48.97	10.75	11.33
H3	7.4	48.92	10.78	11.45
H4	9.09	60.94	9.85	9.8
H4	9.41	58.53	9.87	9.58
H5	9.26	59.56	9.46	9.77
H5	9.75	58.51	9.61	10.02
H6	10.62	63.61	10.74	11.18
H6	11.09	64.44	10.8	11.34

Table 8 – Batch H PCE results from solar simulator over a period of time

This produced the champion value overall of 11.92% PCE.

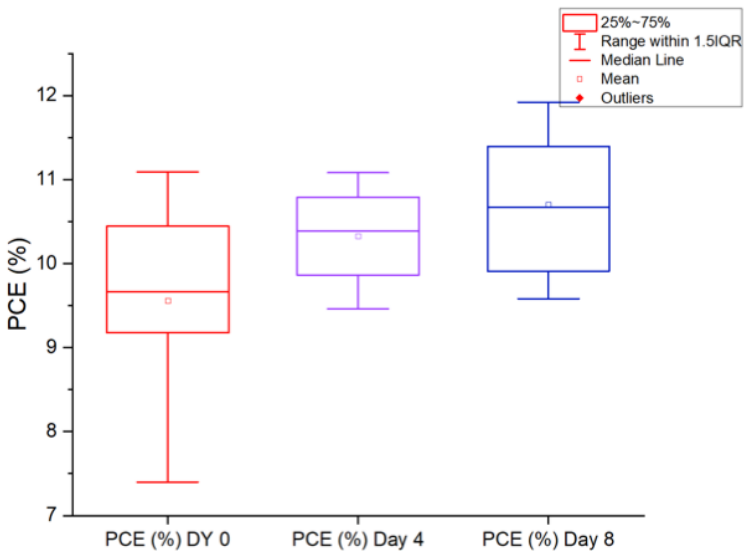

Figure 44 – Box plot of batch H PCE values over time

Figure 44 illustrates the change in the PCE of batch H cells over the course of a week. Between testing sessions on the solar simulator, the cells were kept in a box which aided the stability of the cells.

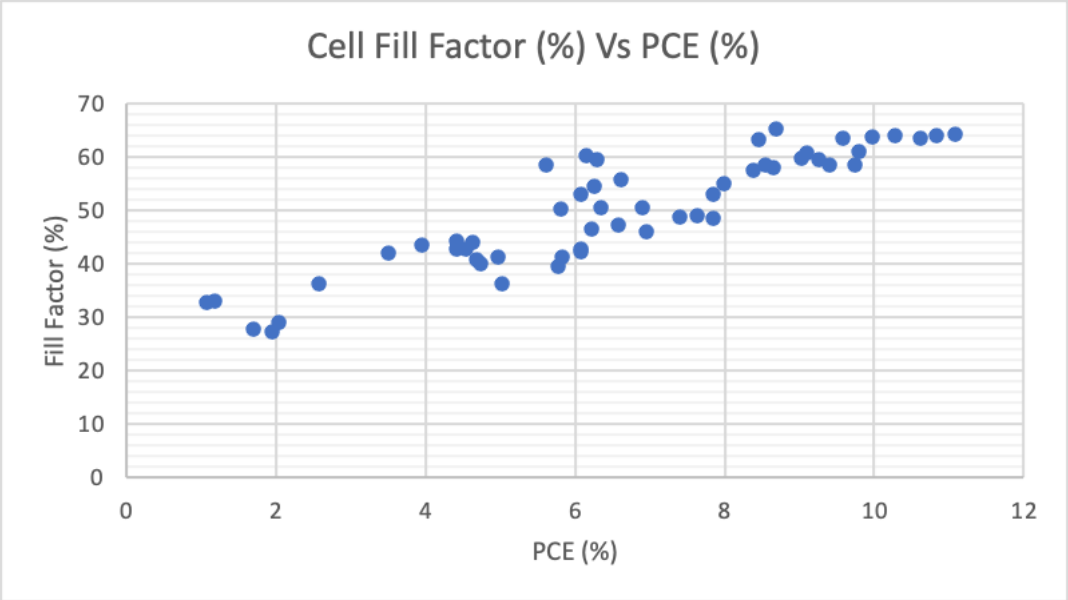

Figure 45 – Graph showing the relationship between fill factor and PCE of cells

The above graph Figure 45 illustrates the influence of the fill factor on the PCE of the modules tested using the solar sim. There is a clear correlation in the data supporting the theory that the higher the fill factor of the cell, the better the PCE.

A challenge that remained even after maximising the stability of the ink by choosing to work exclusively with the GVL solvent based solution was the nozzles clogging on the printhead. This was unavoidable but could be minimised through extensive cleaning before starting the prints to ensure that as many nozzles as possible were working.
This was done using additional GVL solvent which was flushed through the system before filling the ink chamber with the GVL MAPI solution.
Between prints, manual cleaning had to be used which involved wiping the print head with a cloth to remove excess ink that had collected while the inkjet had been jetting.
Reduction of the print area was one approach used to increase the efficiency of the printing process. This meant that a reduced volume of ink was deposited when compared to the original print area of 1cm^2 therefore taking less time to print.
Having more nozzles functional on the printhead also increased efficiency of the process as it reduced the print time.
Gains were made in terms of limiting the overspill from the active area of the cell by reducing the print area. However, there was still some overspill occurring which required additional attention in the post print treatments. To truly optimise the performance of the

inkjet deposition, further work needs to be done so that the overspill is eliminated therefore removing the need for scraping the excess off the surrounding substrate.

The initial rest time post printing used for the cells was 10 minutes. This rest time was the same for the GBL based solution and the GVL based solution.
However, as part of the work done to improve the efficiency of the finished cells this time was extended to 15 minutes when working with the GVL MAPI solution. This extended rest period allowed for additional infiltration of the cell to take place before being placed on the hot plate under accelerated crystallisation/drying conditions.
The cells measured under the solar simulator, that used the GVL based perovskite and rested for the full 15 minutes returned higher efficiency values and increased infiltration compared to the cells that only rested for 10 minutes post printing.

4.7.3 Differences in post print treatment between GBL and GVL

It was a slightly different process for the cells using the GVL solvent system rather than the GBL. This was due to the use of the oven in the low humidity room negatively affecting the efficiency of the cells.

For the GVL system the standard post print procedure was that the cells were infiltrated, then left at room temperature for 10mins to allow a good level of initial infiltration into the stack. They were then placed on a hot plate for 1hour at 45°C (rather than in the oven). They were then transferred to the low humidity oven in the characterisation lab after the hour was up and left there for approx. 24 hours/overnight.

One aspect of the post printing treatment that was targeted as part of testing to reduce the production time of the cells was the 10/15-minute rest at room temperature before the cells were transported to a hot plate to set for one hour after printing. As the print deck of the printer could be heated, tests were run where the cells were placed onto the print deck that was heated to the 45°C. This aimed to eliminate this 15-minute wait time by combining it with the infiltration stage. However, this reduced the time taken for the perovskite to dry meaning that full infiltration of the cell did not occur.

This process was further optimised by leaving the cells for 15 mins, rather than the previously prescribed 10 mins, after printing before placing them on the hotplate. This allowed for further infiltration of the perovskite into the mesoporous stack before the heat of the hot plate accelerated the drying and crystallisation process of the cells.

The only major difference in the post print treatment between the two solvent systems was that when working with the GBL based ink the cells would sit for an hour in an oven whereas when working with the GVL MAPI solution to print the cells were placed on a hot plate in a fume hood in the low humidity room of the lab for 1 hour instead.
All other aspects of the post print treatments and the prep work for solar simulator testing were the same for both inks.

4.7.4 Working on Modules

Initial testing was done on the solar sim with three 5 cm x 5 cm modules.
The deposition for these modules was carried out on the inkjet printer using the same parameters that were optimised as part of the work done in the previous chapters on the 1 cm^2 carbon cells.
While there were some problems with nozzle clogging the inkjet successfully deposited the perovskite onto all three modules demonstrating the possibility of using this technique on a larger scale. The table below compares two modules infiltrated using the standard method with the champion module where the perovskite was deposited into the cell using the inkjet printer.

Cell ID	Direction	Efficiency (%)	Fill Factor (%)	Jsc (mA/Cm≤)	Voc (V) Stabilised
M1 - normal	Forward	0.28	49.48	0.21	2.77
M1 - normal	Reverse	0.13	27.5	0.2	2.42
M2 - normal	Forward	0.17	39.55	0.2	2.11
M2 - normal	Reverse	0.09	28.72	0.19	1.63
M3 - inkjet	Forward	0.05	28.88	0.21	0.89
M3 - inkjet	Reverse	0.04	28.03	0.2	0.77

Table 9 – Results of module testing on the solar simulator

It was not within the scope of this project to work on optimising the performance of the inkjet as a method of deposition for the modules – however this would be the next stage of any future work.

5.0 Conclusion

In conclusion, inkjet printing was found to be a viable method of deposition for the perovskite precursor onto the mesoporous carbon stack. Through optimisation of the piezoelectric wave parameters, and careful management of the print head it was found that it could be used as a manufacturing technique.
The peak time of the wave and the rising edge of the wave, optimised to 17µs and 2µs respectively for the MAPI GVL ink, (Table 4) were the two parameters that had the greatest effect on the performance of the inks. Other parameters were less influential. The inks performed best when operating at ambient temperature.

Another aspect of the process that was optimised through the series of tests was the reproducibility of results. This was important when considering the aim of using the inkjet method in the context of scale-up. For the final solar simulator tests, which returned cells with a champion PCE of 12%, the minimum and maximum values recorded for the efficiency were also only between 1 and 2% of each other meaning there is potential for a highly reproduceable process going forward. This was a significant improvement on previous batches that had much greater variation in the PCEs produced.

Potential drawbacks of this method of deposition include the potential for nozzle clogging when working with the perovskite in the inkjet, as well as the time taken for the whole print and post-print process.

When comparing the two solvent systems, the GVL based perovskite ‘ink’ outperformed the GBL based ‘ink’ in terms of stability when being utilised in the inkjet printer. This led to a much greater focus on the GVL system in the latter portion of the project as it had better capability for longer print runs. This meant that batches of cells could be completed with no jetting issues which was critical to successful deposition and therefore functional solar cells. This is advantageous as the less onerous restrictions placed on the GVL make it more suitable for scaled-up production.

6.0 References

1. *Best Research Cell-Efficiencies, National Renewable Energy Laboratory (NREL)*; April 20 2022, http://www.nrel.gov/ncpv/images/efficiency_chart.jpg.
2. *On the Electro-Optics of Carbon Stack Perovskite Solar Cells;* Robin Kerremans, Oskar J. Sandberg, Simone Meroni, Trystan Watson, Ardalan Armin, Paul Meredith10 July 2019: doi.org/10.1002/solr.201900221
3. *Analytical Review of Spiro-OMeTAD Hole Transport Materials: Paths Toward Stable and Efficient Perovskite Solar Cells*; Laxmi Nakka, Yuanhang Cheng, Armin Gerhard Aberle, Fen Lin; 13 May 2022; doi.org/10.1002/aesr.202200045
4. https://www.iea.org/energy-system/renewables/solar-pv
5. *The Results of Performance Measurements of Field-aged Crystalline Silicon Photovoltaic Modules*; Artur Skoczek, Tony Sample and Ewan D. Dunlop; Progress in Photovoltaics: Research and Applications, Volume 17 Issue 4, 2009, Pages 227 – 240
6. *Best Research Cell-Efficiencies, National Renewable Energy Laboratory (NREL)*, Jan 2022, http://www.nrel.gov/ncpv/images/efficiency_chart.jpg.
7. *The Current Status and Development Trend of Perovskite Solar Cells*; Zhelu Hu, Chenxin Ran, Hui Zhang, Lingfeng Chao, Yonghua Chen, Wei Huang; Journal Engineering; doi.org/10.1016/j.eng.2022.10.012
8. *Green Solvent-Based Perovskite Precursor Development for Ink-Jet Printed Flexible Solar Cells,* Barbara Wilk et al, March 2021 ACS Sustainable Chemistry & Engineering 9(10), DOI:10.1021/acssuschemeng.0c09208
9. *High throughput fabrication of mesoporous carbon perovskite solar cells*; Jenny Baker, Katherine Hooper, Simone Meroni, Adam Pockett, James McGettrick, Zhengfei Wei, Renán Escalante, Gerko Oskam, Matthew Carnie, Trystan Watson; J. Mater. Chem. A, 2017,5, 18643-18650; DOI.org/10.1039/C7TA05674E
10. *Recent progress in inkjet-printed solar cells;* Santhosh Kumar Karunakaran, Gowri Manohari Arumugam, Wentao Yang, Sijie Ge, Saqib Nawaz Khan, Xianzhong Lin, Guowei Yang; *J. Mater. Chem. A*, 2019,7, 13873-13902; DOI: doi.org/10.1039/C9TA03155C
11. *A New Photovoltaic Paradigm: The Silicon-Perovskite Tande*; Mártil, I. (2022); OpenMind BBVA
12. *The Shockley–Queisser limit and the conversion efficiency of silicon-based solar cells*; A.R. Zanatta; doi.org/10.1016/j.rio.2022.100320
13. *Tandems have the power: perovskite-silicon tandem solar cells break the 30% efficiency threshold*; *De Wolf, S. and E. Aydin (2023) Science*, **381**, (6653), 30–31
14. *Best Research-Cell Efficiencies, National Renewable Energy Laboratory, (2020); DOI: 10.1016/j.jet.2007.03.008*
15. *Effect of absorber layer, hole transport layer thicknesses, and its doping density on the performance of perovskite solar cells by device simulation*; Atanu Bag, R. Radhakrishnan, Reza Nekovei, R. Jeyakumar; doi.org/10.1016/j.solener.2019.12.014
16. https://www.nature.com/articles/s41578-024-00678 Perovskite solar cells (PSCs)
17. sciencedirect.com
18. *Metal Oxide Electron Transport Materials For Perovskite Solar Cells: A Review*, K. Valadi et al., Environ. Chem. Lett., 19 (3), 2185–2207 (2021); DOI: 10.1007/s10311-020-01171-x
19. *A Brief Review Of Hole Transporting Materials Commonly Used In Perovskite Solar Cells*, S. Li et al., Rare Met., 40 (10), 2712–2729 (2021); DOI: 10.1007/s12598-020-01691-z
20. *Up-Scalable Sheet-To-Sheet Production Of High Efficiency Perovskite Module And Solar Cells On 6-In. Substrate Using Slot Die Coating*, F. Di Giacomo et al., Sol. Energy Mater. Sol. Cells, 181 (November 2017), 53–59 (2018); DOI: 10.1016/j.solmat.2017.11.010.

21. *Roll-To-Roll Gravure-Printed Flexible Perovskite Solar Cells Using Eco-Friendly Antisolvent Bathing With Wide Processing Window*, Y. Y. Kim et al., Nat. Commun., 11 (1), 1–11 (2020); DOI: 10.1038/s41467-020-18940-5
22. *Absolute energy level positions in tin- and lead-based halide perovskites***;** Shuxia Tao, Ines Schmidt, Geert Brocks, Junke Jiang, Ionut Tranca, Klaus Meerholz, Selina Olthof;Nature Communications volume 10, Article number: 2560 (2019)
23. *The influence of the conduction band engineering on the perovskite solar cell performance;* N. Qasim Agha, Qais Th. Algwari; Results in Optics Dec 2022; https://doi.org/10.1016/j.rio.2022.100291
24. *Stable Triple Cation Perovskite Precursor For Highly Efficient Perovskite Solar Cells Enabled By Interaction With 18C6 Stabilizer*, X. Wu et al., Adv. Funct. Mater., 30 (6), (2020); DOI: 10.1002/adfm.201908613
25. *Cesium-Containing Triple Cation Perovskite Solar Cells: Improved Stability, Reproducibility And High Efficiency*, M. Saliba et al., Energy Environ. Sci., 9 (6), 1989–1997 (2016); DOI:10.1039/C5EE03874J
26. *Fully Spray-Coated Triple-Cation Perovskite Solar Cells*, J. E. Bishop et al., Sci. Rep., 10 (1), 1–8 (2020); DOI: 10.1038/s41598-020-63674-5
27. *Ambient Air Blade-Coating Fabrication Of Stable Triple-Cation Perovskite Solar Modules By Green Solvent Quenching*, L. Vesce et al., Sol. RRL, 5 (8), 1–11 (2021); DOI: 10.1002/solr.202100073
28. *High-Performance Perovskite Single-Junction And Textured Perovskite/Silicon Tandem Solar Cells Via Slot-Die Coating*, A. S. Subbiah et al., ACS Energy Lett., 5 (9), 3034–3040 (2020); DOI: 10.1021/acsenergylett.0c01297
29. *Metal Oxide Electron Transport Materials For Perovskite Solar Cells: A Review*, K. Valadi et al., Environ. Chem. Lett., 19 (3), 2185–2207 (2021); DOI: 10.1007/s10311-020-01171-x
30. *Formamidinium Lead Trihalide: A Broadly Tunable Perovskite For Efficient Planar Heterojunction Solar Cells*, G. E. Eperon et al., Energy Environ. Sci., 7 (3), 982 (2014); DOI: 10.1039/c3ee43822h
31. *Perovskite Solar Cells With Atomically Coherent Interlayers On SnO2 Electrodes*, H. Min et al., Nature, 598 (7881), 444–450 (2021); DOI: 10.1038/s41586-021-03964-8
32. *Lead Halide–Templated Crystallization Of Methylamine-Free Perovskite For Efficient Photovoltaic Modules*, T. Bu et al., Science (80-.)., 372 (6548), 1327–1332 (2021); DOI: 10.1126/science.abh1035
33. *Slot-Die Coating Large-Area Formamidinium-Cesium Perovskite Film For Efficient And Stable Parallel Solar Module*, Z. Yang et al., Sci. Adv., 7 (18), 1–14 (2021); DOI: 10.1126/sciadv.abg3749
34. *Stable Perovskite Solar Cells With Efficiency Exceeding 24.8% And 0.3-V Voltage Loss*, M. Jeong et al., Science (80-.)., 369 (6511), 1615–1620 (2020); DOI: 10.1126/science.abb7167
35. *Metal Oxide Electron Transport Materials For Perovskite Solar Cells: A Review, K. Valadi et al., Environ. Chem. Lett., 19 (3), 2185–2207 (2021); DOI: 10.1007/s10311-020-01171-x.*
36. *Impact of Perovskite Composition on Film Formation Quality and Photophysical Properties for Flexible Perovskite Solar Cells*; Guangdong Li, Xiaoping Zou, Jin Cheng, Dan Chen, Yujun Yao, Chuangchuang Chang, Xing Yu, Zixiao Zhou, Junqi Wang, and Baoyu Liu; Solar Energy Volume 196, 15 January 2020; doi.org: 10.1016/j.solener.2019.12.014
37. *Up-Scalable Sheet-To-Sheet Production Of High Efficiency Perovskite Module And Solar Cells On 6-In. Substrate Using Slot Die Coating*, F. Di Giacomo et al., Sol. Energy Mater. Sol. Cells, 181 (November 2017), 53–59 (2018); DOI: 10.1016/j.solmat.2017.11.010
38. *Roll-To-Roll Gravure-Printed Flexible Perovskite Solar Cells Using Eco-Friendly Antisolvent Bathing With Wide Processing Window*, Y. Y. Kim et al., Nat. Commun., 11 (1), 1–11 (2020); DOI: 10.1038/s41467-020-18940-5
39. *Inkjet printed mesoscopic perovskite solar cells with custom design capability,* Anand Verma et al, Mater.Adv., 2020, 1, 153-160, DOI: 10.1039/D0MA00077A
40. *How additives for tin halide perovskites influence the Sn4+ concentration,* Aaron J Huckaba et al, J. Mater. Chem. A, 2022,**10**, 13278-13285, DOI: 10.1039/D2TA01429G
41. *Air Processed Inkjet Infiltrated Carbon Based Printed Perovskite Solar Cells with High Stability and Reproducibility*; S. G. Hashmi, D. Martineau, X. Li, M. Ozkan, A. Tiihonen, M. I. Dar, T. Sarikka, S. M. Zakeeruddin, J. Paltakari, P. D. Lund and M. Gratzel, Adv. Mater. Technol., 2017, 2, 1600183.

42. SUSS website https://www.suss.com/en/products-solutions/inkjet-printing
43. *Evaluation of Inkjet Technologies for Digital Fabrication & Functional Printing*; Vincent Cahill, Dene Taylor; *Proc.* IS&T Int'l Conf. on Digital Printing Technologies and Digital Fabrication (NIP28), 2012, pp 315 - 317, DOI: 10.2352/ISSN.2169-4451.2012.28.1.art00012_2
44. https://www.gov.uk/government/publications/circular-0042022-gamma-butyrolactone-gbl-and-14-butanediol-14-bd-revocation-of-rescheduling/circular-0042022-gamma-butyrolactone-gbl-and-14-butanediol-14-bd-revocation-of-rescheduling
45. *γ-Valerolactone: A Nontoxic Green Solvent for Highly Stable Printed Mesoporous Perovskite Solar Cells,* Carys Worsley et al. 2021, Energ Tech., DOI:10.1002/ente.202100312
46. *Spontaneous enhancement of the stable power conversion efficiency in perovskite solar cells*; Somayeh Moghadamzadeh, Ihteaz M. Hossain, Marius Jakoby, Bahram Abdollahi Nejand, Diana Rueda-Delgado, Jonas A. Schwenzer, Saba Gharibzadeh, Tobias Abzieher, Motiur Rahman Khan, Amir A. Haghighirad, Ian A. Howard, Bryce S. Richards, Uli Lemmer and Ulrich W. Paetzold; J. Mater. Chem. A, 2020,8, 670-682; DOI: doi.org/10.1039/C9TA09584E